

Electronic Supplementary Information

Brominated [20]silafulleranes: pushing the limits of steric loading

*Marcel Bamberg, Thomas Gasevic, Michael Bolte, Alexander Virovets, Hans-Wolfram Lerner, Stefan Grimme, Markus Bursch, Matthias Wagner**

Content:

1. General experimental procedures.....	S2
2. Siladodecahedranes: Syntheses and characterization data.....	S3
2.1. Synthesis of $[n\text{Bu}_4\text{N}][\text{Cl}@Si_{20}(\text{SiBr}_2\text{H})_{12}\text{Br}_8]$ ($[n\text{Bu}_4\text{N}][\mathbf{2}]$).....	S4
2.2. Synthesis of $[n\text{Bu}_4\text{N}][\text{Cl}@Si_{20}(\text{SiBr}_3)_{12}\text{Br}_8]$ ($[n\text{Bu}_4\text{N}][\mathbf{3}]$).....	S6
2.3. Synthesis of $[n\text{Bu}_4\text{N}][\text{Cl}@Si_{20}(\text{SiH}_3)_{12}\text{Br}_8]$ ($[n\text{Bu}_4\text{N}][\mathbf{4}]$).....	S7
3. Plots of NMR spectra.....	S8
3.1. NMR spectra of $[n\text{Bu}_4\text{N}][\mathbf{2}]$	S8
3.2. NMR spectra of $[n\text{Bu}_4\text{N}][\mathbf{3}]$	S12
3.3. NMR spectra of $[n\text{Bu}_4\text{N}][\mathbf{4}]$	S14
4. Plots of mass spectra.....	S18
5. X-ray crystal structure analyses.....	S25
6. Computational details.....	S32
6.1. General remarks and geometry optimizations.....	S32
6.2. Calculation of NMR shifts.....	S32
6.3. Scaling of calculated ^{35}Cl chemical shift values.....	S33
7. References.....	S34

1. General experimental procedures

All reactions and manipulations were carried out under exclusion of air and moisture using Schlenk techniques or a glovebox.

$[n\text{Bu}_4\text{N}][\text{Cl}@\text{Si}_{20}(\text{SiH}_3)_{12}\text{H}_8]$ ($[n\text{Bu}_4\text{N}][\mathbf{1}]$) was synthesized according to the published procedure.^{S1} *n*-Hexane was distilled from Na metal; Et₂O and THF were distilled from Na/benzophenone prior to use. CH₂Cl₂ was distilled from CaH₂. 1,2-Difluorobenzene (*o*DFB) was dried over CaH₂, transferred via gas phase into a J. Young vessel, degassed by three freeze-pump-thaw cycles, and stored over molecular sieves (3 Å). C₆D₁₂ was dried over molecular sieves (3 Å). BBr₃ was stored over Hg. *i*Bu₂AlH (1.0 M in cyclohexane) was purchased from *Sigma-Aldrich* and used as received.

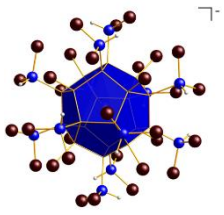
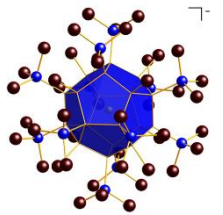
NMR spectra were recorded at 298 K using Bruker Avance III 500 HD or DPX 250 spectrometers. Chemical shift values are referenced to (residual) solvent signals (¹H/¹³C{¹H}); THF-*d*₈: $\delta = 3.58/67.21$;^{S2} C₆D₁₂ in *o*DFB (1:5): $\delta = 1.34/26.48$ ^{S3}) or to external standards (²⁹Si/²⁹Si{¹H}: Si(CH₃)₄; ³⁵Cl/³⁵Cl{¹H}: NaCl in D₂O). Abbreviations: s = singlet, d = doublet, t = triplet, q = quartet, m = multiplet, br = broad, n. o. = not observed, n. r. = not resolved, *h*_{1/2} = full width at half maximum.

IR spectra were recorded using a *JASCO* FT/IR-4200 spectrometer equipped with a *PIKE* Technologies GladiATR unit. Multiple scans per measurement were accumulated to increase the signal-to-noise ratio. Abbreviations: s = strong signal, m = medium signal, w = weak signal, br = broad.

LDI-MS spectra were recorded on a MALDI LTQ Orbitrap XL (*Thermo Fisher Scientific*) in the negative ion mode. The resolution was set to 60000. The sample spots were prepared inside a glovebox: A suspension of the finely ground sample in Et₂O was transferred to the sample holder by a transfer pipette to form a thin layer of material after evaporation. A nitrogen-filled desiccator was used to take the sample holder from the inside of the glovebox to the mass spectrometer. In a typical experiment, the laser energy was set to 50 μJ and at least 20 to 30 spectra were accumulated to increase the signal-to-noise ratio. The isotope patterns of selected ion species were compared to the theoretical pattern calculated from the elemental composition of the anions using the software *mMass*.^{S4-6}

2. Siladodecahedranes: Syntheses and characterization data

Table S1. Numbering scheme, X-ray crystal structure plots, and selected NMR spectroscopic parameters of the silafullerane anions **[2]⁻**, **[3]⁻**, and **[4]⁻**. NMR spectroscopic data are given for the $[n\text{Bu}_4\text{N}]^+$ salts and were acquired in *o*DFB/*C*₆D₁₂ mixtures (5:1).

	[2]⁻	[3]⁻	[4]⁻
solid-state structure			---
chemical formula	$[\text{Cl}@Si_{20}(\text{SiBr}_2\text{H})_{12}\text{Br}_8]^-$	$[\text{Cl}@Si_{20}(\text{SiBr}_3)_{12}\text{Br}_8]^-$	$[\text{Cl}@Si_{20}(\text{SiH}_3)_{12}\text{Br}_8]^-$
$\delta(^1\text{H})$	5.79	---	3.73
$\delta(^{29}\text{Si})$	17.1 (<i>SiBr</i>) -63.1 (<i>Si⁰</i>) -7.9 (<i>SiBr₂H</i>)	n. o.	35.4 (<i>SiBr</i>) -68.1 (<i>Si⁰</i>) -93.9 (<i>SiH₃</i>)
$^1J(\text{Si},\text{H})$ [Hz]	284.6	---	203.4
$\delta(^{35}\text{Cl})$	308.7	271.2	373.0

2.1. Synthesis of $[n\text{Bu}_4\text{N}][\text{Cl}@\text{Si}_{20}(\text{SiBr}_2\text{H})_{12}\text{Br}_8]$ ($[n\text{Bu}_4\text{N}][\mathbf{2}]$)

Neat BBr_3 (0.20 mL, 2.1 mmol, ≈ 120 eq) was added at room temperature to a stirred suspension of $[n\text{Bu}_4\text{N}][\mathbf{1}]$ (22 mg, 18 μmol , 1.0 eq) in *o*DFB (2.5 mL). Within a few minutes, the suspension turned into a clear colorless solution, which was stirred for a total of 30 min after the addition of BBr_3 . A dynamic vacuum was applied for 30 min to remove all volatile components. Since the product deposited on the glass wall of the reaction vessel, *n*-hexane (1.0 mL) was added and the sample was placed in an ultrasonic bath until a colorless suspension formed. A dynamic vacuum was again applied to obtain $[n\text{Bu}_4\text{N}][\mathbf{2}]$ (66 mg, 18 μmol , $>90\%$) as colorless powder.

^1H NMR (500.2 MHz, *o*DFB/ C_6D_{12} 5:1): $\delta = 5.79$ (s, 12H; SiBr_2H), 3.15–3.12 (m, 8H, $\text{N}-\text{CH}_2$), 1.69–1.63 (m, 8H, $\text{N}-\text{CH}_2-\text{CH}_2$), 1.45–1.37 (m, 8H, CH_2-CH_3), 0.96 (t, $^3J(\text{H},\text{H}) = 7.4$ Hz, 12H, CH_3).

$^{13}\text{C}\{^1\text{H}\}$ NMR (125.8 MHz, *o*DFB/ C_6D_{12} 5:1): $\delta = 59.9$ ($\text{N}-\text{CH}_2$), 24.5 ($\text{N}-\text{CH}_2-\text{CH}_2$), 20.4 (CH_2-CH_3), 13.6 (CH_2-CH_3).

^{29}Si NMR (99.4 MHz, *o*DFB/ C_6D_{12} 5:1): $\delta = 17.1$ (s, SiBr), -7.9 (d, $^1J(\text{Si},\text{H}) = 284.6$ Hz, SiBr_2H), -63.1 (d, $^2J(\text{Si},\text{H}) = 20.5$ Hz, Si^0).

$^{29}\text{Si}\{^1\text{H}\}$ NMR (99.4 MHz, *o*DFB/ C_6D_{12} 5:1): $\delta = 17.1$ (SiBr), -7.9 (SiBr_2H), -63.1 (Si^0).

$^{35}\text{Cl}\{^1\text{H}\}$ NMR (49.0 MHz, *o*DFB/ C_6D_{12} 5:1): $\delta = 308.7$ (s, $h_{1/2} \approx 31$ Hz, endohedral Cl).

LDI-MS(-): $m/z =$ selected peaks: 3393.67 ($[\text{Cl}@\text{Si}_{31}\text{H}_{11}\text{Br}_{31}]^-$, calcd.: 3393.77), 3313.73 ($[\text{Cl}@\text{Si}_{31}\text{H}_{12}\text{Br}_{30}]^-$, calcd.: 3313.86), 3237.82 ($[\text{Cl}@\text{Si}_{31}\text{H}_{13}\text{Br}_{29}]^-$, calcd.: 3237.95), 3203.85 ($[\text{Cl}@\text{Si}_{30}\text{H}_{11}\text{Br}_{29}]^-$, calcd.: 3203.96), 3124.93 ($[\text{Cl}@\text{Si}_{30}\text{H}_{11}\text{Br}_{28}]^-$, calcd.: 3125.04), 3016.04 ($[\text{Cl}@\text{Si}_{29}\text{H}_9\text{Br}_{27}]^-$, calcd.: 3016.13), 2936.12 ($[\text{Cl}@\text{Si}_{29}\text{H}_8\text{Br}_{26}]^-$, calcd.: 2936.21), 2910.14 ($[\text{Cl}@\text{Si}_{28}\text{H}_{10}\text{Br}_{26}]^-$, calcd.: 2910.25), 2830.23 ($[\text{Cl}@\text{Si}_{28}\text{H}_{11}\text{Br}_{25}]^-$, calcd.: 2830.34), 2560.51 ($[\text{Cl}@\text{Si}_{27}\text{H}_{10}\text{Br}_{22}]^-$, calcd.: 2560.60).

IR (ATR): $\tilde{\nu}(\text{Si}-\text{H}) = 2177$ cm^{-1} (w).

Notes:

- *Synthesis*: According to ^{11}B NMR spectroscopy, HBBr_2 is the main byproduct of the H/Br exchange.
- *Crystallization protocol*: An NMR tube was charged with $[\text{nBu}_4\text{N}][\mathbf{1}]$ (10 mg, $8.0\ \mu\text{mol}$, 1.0 eq), *o*DFB (0.50 mL), and BBr_3 (0.10 mL, 1.0 mmol, ≈ 120 eq). The sample was flame-sealed and investigated by $^{35}\text{Cl}\{^1\text{H}\}$ NMR spectroscopy to confirm the formation of $[\text{nBu}_4\text{N}][\mathbf{2}]$. Subsequently, the sample was stored in a freezer at $-30\ ^\circ\text{C}$. After 18 d, colorless crystals of $[\text{nBu}_4\text{N}][\mathbf{2}]$ were harvested and investigated by SC-XRD.
- *^{29}Si NMR spectrum*: The $\delta(^{29}\text{Si})$, $^1J(\text{H},\text{Si})$, and $^2J(\text{H},\text{Si})$ values of the SiBr_2H groups in $[\text{nBu}_4\text{N}][\mathbf{2}]$ and those reported by Hassler and Bauer for SiBr_2H -/ SiBrH_2 -containing disilanes are compared in Table S2.^{S7}

Table S2. Selected NMR-spectroscopic data of representative SiBr_2H - and SiBrH_2 -containing disilanes^{S7} in comparison with those of the silafullerane $[\text{nBu}_4\text{N}][\mathbf{2}]$.

Compound	$\delta(^{29}\text{Si})$ (Si)	$^1J(\underline{\text{H}},\underline{\text{Si}})$ [Hz]	$^2J(\underline{\text{H}},\underline{\text{Si}})$ [Hz]
$\text{Br}\underline{\text{H}_2}\underline{\text{Si}}-\text{SiH}_3$	-42.3	226.9	12.2
$\text{Br}\underline{\text{H}_2}\underline{\text{Si}}-\text{SiH}_2\text{Br}$	-45.2	235.7	15.1
$\text{Br}\underline{\text{H}_2}\underline{\text{Si}}-\text{SiHBr}_2$	-43.9	243.1	19.7
$\text{Br}\underline{\text{H}_2}\underline{\text{Si}}-\text{SiBr}_3$	-40.1	249.0	26.0
$\text{Br}_2\underline{\text{HSi}}-\text{SiH}_3$	5.0	264.7	21.1
$\text{Br}_2\underline{\text{HSi}}-\text{SiH}_2\text{Br}$	-21.1	275.5	26.5
$\text{Br}_2\underline{\text{HSi}}-\text{SiHBr}_2$	-24.8	293.1	33.1
$\text{Br}_2\underline{\text{HSi}}-\text{SiBr}_3$	-24.9	290.3	43.8
$[\text{nBu}_4\text{N}][\mathbf{2}]$ ($\text{Br}_2\underline{\text{HSi}}$)	-7.9	284.6	20.5

2.2. Synthesis of $[n\text{Bu}_4\text{N}][\text{Cl}@\text{Si}_{20}(\text{SiBr}_3)_{12}\text{Br}_8]$ ($[n\text{Bu}_4\text{N}][\mathbf{3}]$)

An NMR tube was charged with $[n\text{Bu}_4\text{N}][\mathbf{1}]$ (4 mg, 3 μmol , 1 eq), C_6D_{12} (0.10 mL), BBr_3 (0.10 mL, 1.1 mmol, ≈ 300 eq), and *o*DFB (0.50 mL). The sample was flame-sealed, placed in a sand bucket, and heated to 130 $^\circ\text{C}$ for 3 d in an oven. After the oven had been turned off, its door was kept closed for another 3 d to allow the sample (in the sand bucket) to cool down very slowly. Subsequently, the NMR tube, which contained a slightly orange solution and a few colorless, needle-shaped crystals, was opened inside a glovebox to pick the single crystals of $[n\text{Bu}_4\text{N}][\mathbf{3}]$. Due to the poor solubility of $[n\text{Bu}_4\text{N}][\mathbf{3}]$, a ^{29}Si NMR spectrum could not be obtained within a reasonable measurement time.

^1H NMR (500.2 MHz, *o*DFB/ C_6D_{12} 5:1): δ = 3.15–3.11 (m, 8H, N– CH_2), 1.70–1.64 (m, N– CH_2 – CH_2), 1.44–1.38* (m, CH_2 – CH_3), 0.96 (t, $^3J(\text{H},\text{H}) = 7.3$ Hz, 12H, CH_3). *Superposition with the solvent signal at 1.34 ppm.

$^{13}\text{C}\{^1\text{H}\}$ NMR (125.8 MHz, *o*DFB/ C_6D_{12} 5:1): δ = 59.9 (N– CH_2), 24.5 (N– CH_2 – CH_2), 20.4 (CH_2 – CH_3), 13.5 (CH_2 – CH_3).

^{35}Cl NMR (49.0 MHz, *o*DFB/ C_6D_{12} 5:1): δ = 271.2 (s, $h_{\nu_2} \approx 9$ Hz, endohedral Cl).

LDI-MS(–): m/z = selected peaks: 3349.63 ($[\text{Cl}@\text{Si}_{27}\text{Br}_{32}]^-$, calcd.: 3349.70), 3323.64 ($[\text{Cl}@\text{Si}_{26}\text{Br}_{32}]^-$, calcd.: 3323.72), 3349.63 ($[\text{Cl}@\text{Si}_{27}\text{Br}_{32}]^-$, calcd.: 3349.70), 3191.79 ($[\text{Cl}@\text{Si}_{27}\text{Br}_{30}]^-$, calcd.: 3191.86), 3163.82 ($[\text{Cl}@\text{Si}_{27}\text{Br}_{30}]^-$, calcd.: 3163.89), 3133.84 ($[\text{Cl}@\text{Si}_{27}\text{Br}_{30}]^-$, calcd.: 3133.91), 3003.98 ($[\text{Cl}@\text{Si}_{26}\text{Br}_{28}]^-$, calcd.: 3004.05), 2974.01 ($[\text{Cl}@\text{Si}_{25}\text{Br}_{28}]^-$, calcd.: 2974.07), 2948.03 ($[\text{Cl}@\text{Si}_{24}\text{Br}_{28}]^-$, calcd.: 2948.10), 2868.12 ($[\text{Cl}@\text{Si}_{24}\text{Br}_{27}\text{H}]^-$, calcd.: 2868.19), 2816.18 ($[\text{Cl}@\text{Si}_{25}\text{Br}_{26}]^-$, calcd.: 2816.24), 2788.20 ($[\text{Cl}@\text{Si}_{24}\text{Br}_{26}]^-$, calcd.: 2788.26), 2760.22 ($[\text{Cl}@\text{Si}_{23}\text{Br}_{26}]^-$, calcd.: 2760.28), 2626.37 ($[\text{Cl}@\text{Si}_{24}\text{Br}_{24}]^-$, calcd.: 2626.43), 2600.40 ($[\text{Cl}@\text{Si}_{23}\text{Br}_{24}]^-$, calcd.: 2600.45), 2570.42 ($[\text{Cl}@\text{Si}_{22}\text{Br}_{24}]^-$, calcd.: 2570.47), 2492.51 ($[\text{Cl}@\text{Si}_{22}\text{Br}_{23}\text{H}]^-$, calcd.: 2492.56), 2410.59 ($[\text{Cl}@\text{Si}_{22}\text{Br}_{22}]^-$, calcd.: 2410.64), 2382.62 ($[\text{Cl}@\text{Si}_{21}\text{Br}_{22}]^-$, calcd.: 2382.66), 294.68 ($[\text{Si}_2\text{Br}_3]^-$, calcd.: 294.71).

2.3. Synthesis of $[n\text{Bu}_4\text{N}][\text{Cl}@\text{Si}_{20}(\text{SiH}_3)_{12}\text{Br}_8]$ ($[n\text{Bu}_4\text{N}][\mathbf{4}]$)

A solution of $i\text{Bu}_2\text{AlH}$ in C_6H_{12} (0.18 mL, 1.0 M, 0.18 mmol, 30 eq) was evaporated under a dynamic vacuum and the remaining oily $i\text{Bu}_2\text{AlH}$ was dissolved in a mixture of $o\text{DFB}$ (0.5 mL) and Et_2O (0.5 mL). This solution was added at room temperature to a flask containing $[n\text{Bu}_4\text{N}][\mathbf{2}]$ (22 mg, 5.9 μmol , 1.0 eq) and the clear, colorless reaction mixture was stirred for 16 h. The product was precipitated by addition of n -hexane (5 mL) to the reaction solution. The liquid phase was filtered off and the solid residue was washed with n -hexane (2 mL) and dried under a dynamic vacuum. $[n\text{Bu}_4\text{N}][\mathbf{4}]$ was obtained as a colorless powder (5 mg, 2 μmol , $\approx 35\%$).

^1H NMR (500.2 MHz, $o\text{DFB}/\text{C}_6\text{D}_{12}$ 5:1): $\delta = 3.73$ (s, SiH_3), 3.12 (br, $\text{N}-\text{CH}_2$), 1.66 (br, $\text{N}-\text{CH}_2-\text{CH}_2$), 1.46–1.39 (br, CH_2-CH_3), 0.96 (br, CH_3).

Note: The signals of $[n\text{Bu}_4\text{N}]^+$ were strongly broadened and showed inaccurate integral ratios when measured in $o\text{DFB}/\text{C}_6\text{D}_{12}$ (5:1). When measured in $\text{THF}-d_8$, the expected multiplets were resolved, but $[\mathbf{4}]^-$ decomposed (cf. Figs. S13 and S14).

$^{13}\text{C}\{^1\text{H}\}$ NMR (125.8 MHz, $o\text{DFB}/\text{C}_6\text{D}_{12}$ 5:1): $\delta = 59.9$ ($\text{N}-\text{CH}_2$), 24.6 ($\text{N}-\text{CH}_2-\text{CH}_2$), 20.5 (CH_2-CH_3), 13.7 (CH_3).

$^{29}\text{Si}\{^1\text{H}\}$ NMR (99.4 MHz, $o\text{DFB}/\text{C}_6\text{D}_{12}$ 5:1): $\delta = -94.1$ (SiH_3).

Due to the low signal-to-noise ratio of the $^{29}\text{Si}\{^1\text{H}\}$ NMR spectrum (Fig. S16), two of three signals were only detectable by $^1\text{H}^{29}\text{Si}$ -HMBC and HSQC experiments:

$^1\text{H}^{29}\text{Si}$ -HMBC NMR (500.2 / 99.4 MHz, $o\text{DFB}/\text{C}_6\text{D}_{12}$ 5:1): $\delta = \{3.7, 35.4\}$ ($\text{SiH}_3 / \text{SiBr}$), $\{3.7, -68.1\}$ ($\text{SiH}_3 / \text{Si}^0$), $\{3.7, -93.9\}$ ($\text{SiH}_3 / \text{SiH}_3$).

$^1\text{H}^{29}\text{Si}$ -HSQC NMR (500.2 / 99.4 MHz, $o\text{DFB}/\text{C}_6\text{D}_{12}$ 5:1): $\delta = \{3.7, -93.9\}$ ($\text{SiH}_3 / \text{SiH}_3$).

$^{35}\text{Cl}\{^1\text{H}\}$ NMR (49.0 MHz, $o\text{DFB}/\text{C}_6\text{D}_{12}$ 5:1): $\delta = 372.9$ (s, $h_{1/2} \approx 10$ Hz, endohedral Cl).

LDI-MS(-): $m/z =$ molecular-ion peak: 1609.82 ($[\text{Cl}@\text{Si}_{32}\text{H}_{36}\text{Br}_8]^-$, calcd.: 1609.85); selected additional peaks: 1767.62 ($[\text{Cl}@\text{Si}_{32}\text{H}_{34}\text{Br}_{10}]^-$, calcd.: 1767.67), 1687.72 ($[\text{Cl}@\text{Si}_{32}\text{H}_{35}\text{Br}_9]^-$, calcd.: 1687.76), 1657.73 ($[\text{Cl}@\text{Si}_{31}\text{H}_{33}\text{Br}_9]^-$, calcd.: 1657.76), 1579.82 ($[\text{Cl}@\text{Si}_{31}\text{H}_{34}\text{Br}_8]^-$, calcd.: 1579.85), 1549.83 ($[\text{Cl}@\text{Si}_{30}\text{H}_{32}\text{Br}_8]^-$, calcd.: 1549.86), 1529.91 ($[\text{Cl}@\text{Si}_{32}\text{H}_{37}\text{Br}_7]^-$, calcd.: 1529.94), 1499.92 ($[\text{Cl}@\text{Si}_{31}\text{H}_{35}\text{Br}_7]^-$, calcd.: 1499.95), 1469.93 ($[\text{Cl}@\text{Si}_{30}\text{H}_{33}\text{Br}_7]^-$, calcd.: 1469.95).

IR (ATR): $\tilde{\nu}(\text{Si}-\text{H}) = 2136 \text{ cm}^{-1}$ (m).

3. Plots of NMR spectra

3.1. NMR spectra of $[n\text{Bu}_4\text{N}][2]$

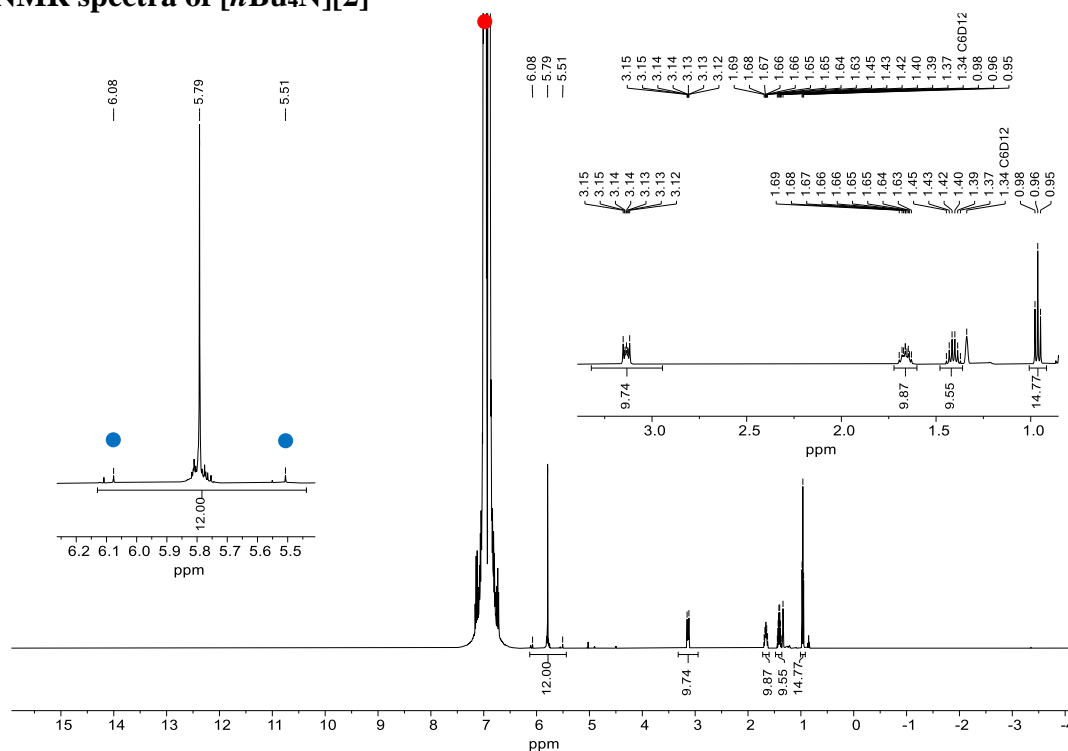


Figure S1. ^1H NMR spectrum (500.2 MHz, $o\text{DFB}/\text{C}_6\text{D}_{12}$ 5:1) of $[n\text{Bu}_4\text{N}][2]$. ^{29}Si satellites are marked with blue dots, the solvent signal of $o\text{DFB}$ is marked with a red dot.

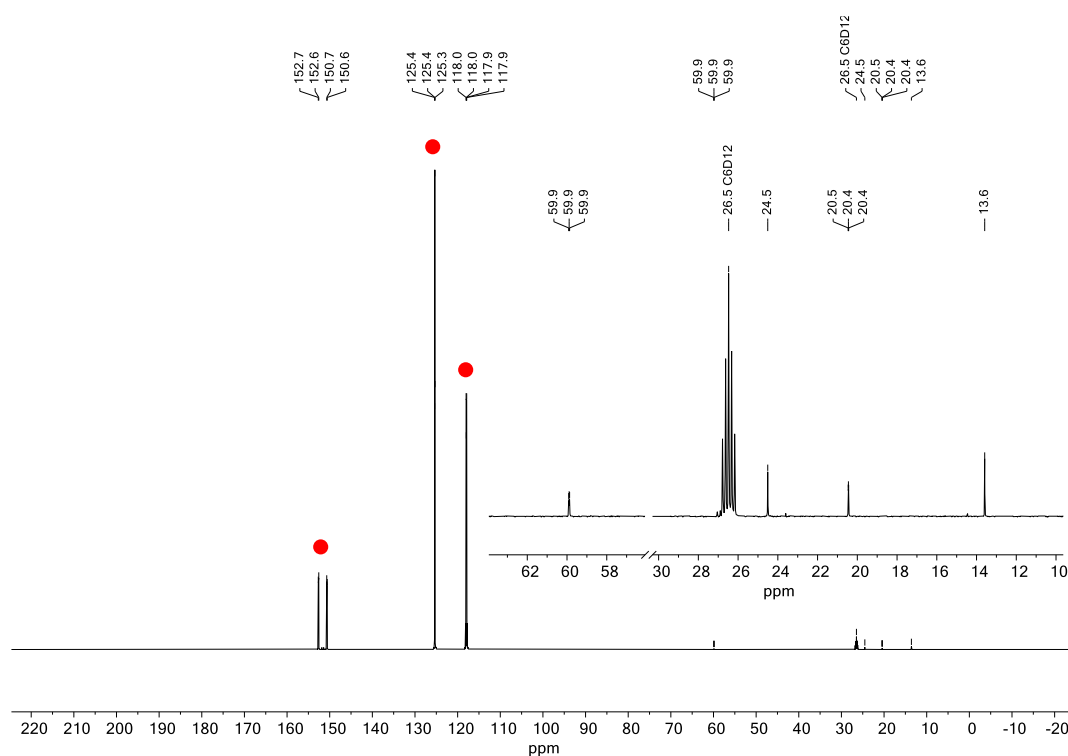


Figure S2. $^{13}\text{C}\{^1\text{H}\}$ NMR spectrum (125.8 MHz, $o\text{DFB}/\text{C}_6\text{D}_{12}$ 5:1) of $[n\text{Bu}_4\text{N}][2]$. The solvent signals of $o\text{DFB}$ are marked with red dots.

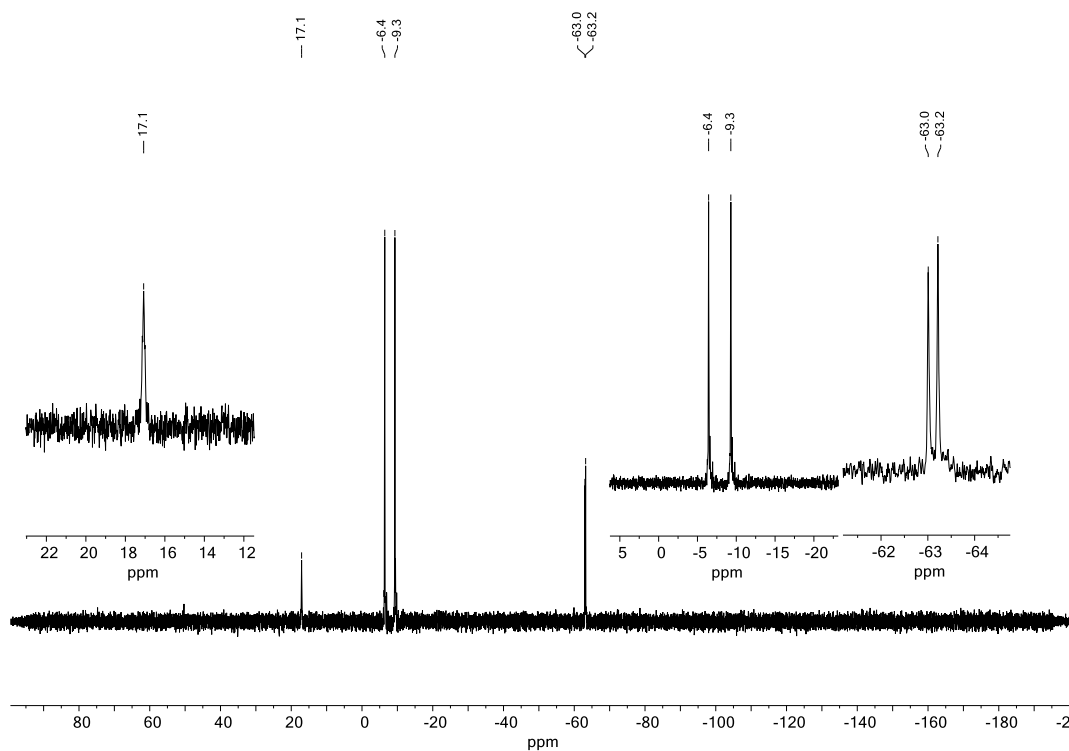


Figure S3. ^{29}Si NMR spectrum (99.4 MHz, *o*DFB/ C_6D_{12} 5:1) of $[\text{nBu}_4\text{N}][\mathbf{2}]$.

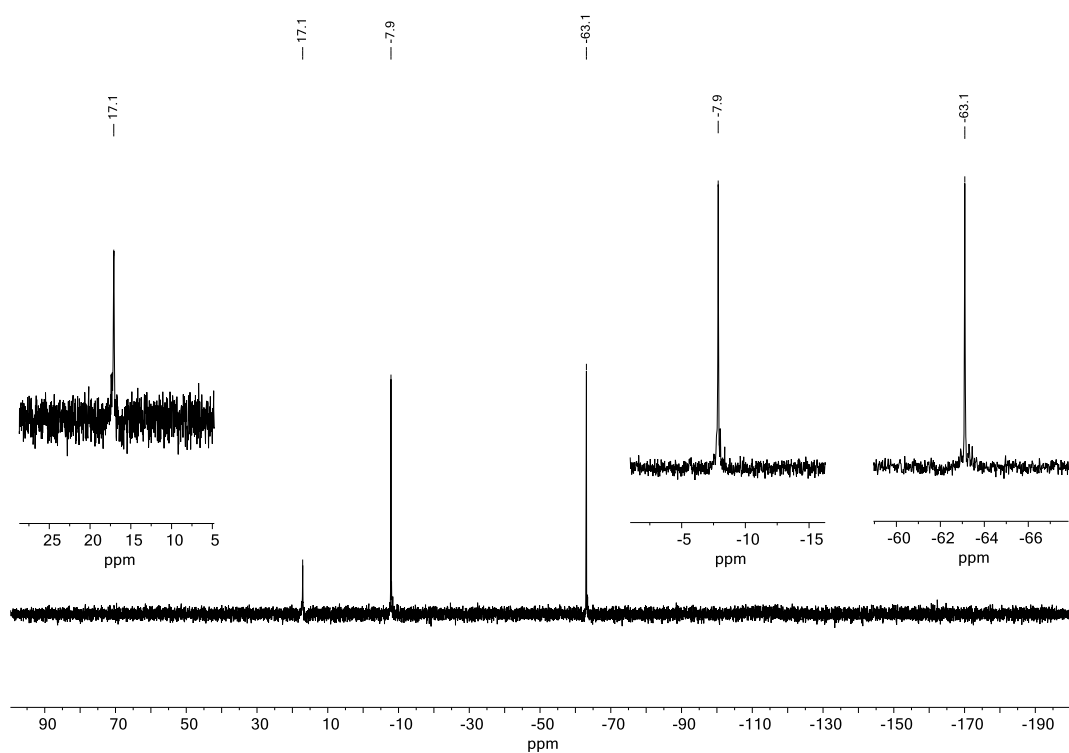


Figure S4. $^{29}\text{Si}\{^1\text{H}\}$ NMR spectrum (99.4 MHz, *o*DFB/ C_6D_{12} 5:1) of $[\text{nBu}_4\text{N}][\mathbf{2}]$.

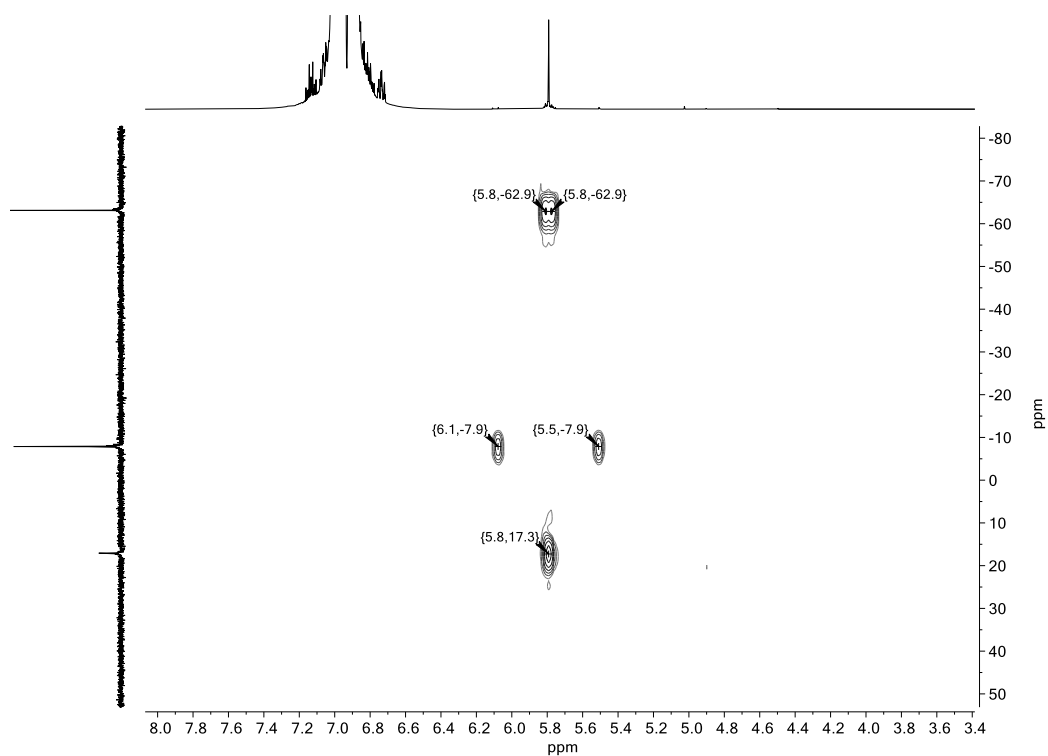


Figure S5. $^1\text{H}^{29}\text{Si}$ -HMBC NMR spectrum (500.2 / 99.4 MHz, *o*DFB/ C_6D_{12} 5:1) of $[\text{nBu}_4\text{N}][\mathbf{2}]$.

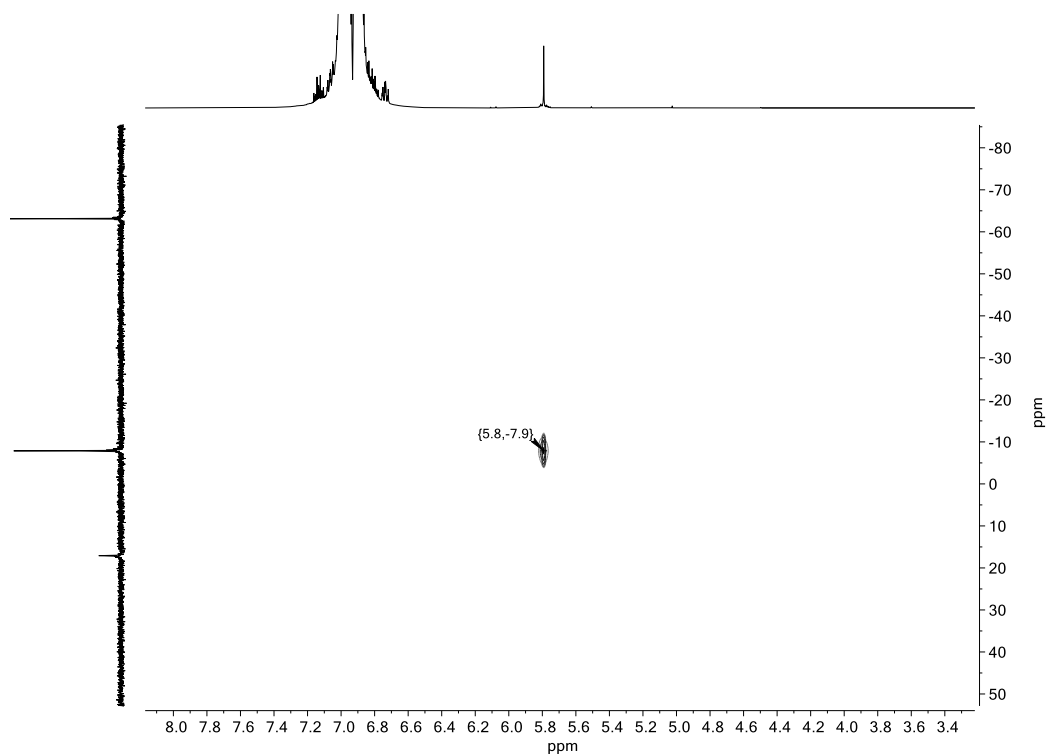


Figure S6. $^1\text{H}^{29}\text{Si}$ -HSQC NMR spectrum (500.2 / 99.4 MHz, *o*DFB/ C_6D_{12} 5:1) of $[\text{nBu}_4\text{N}][\mathbf{2}]$.

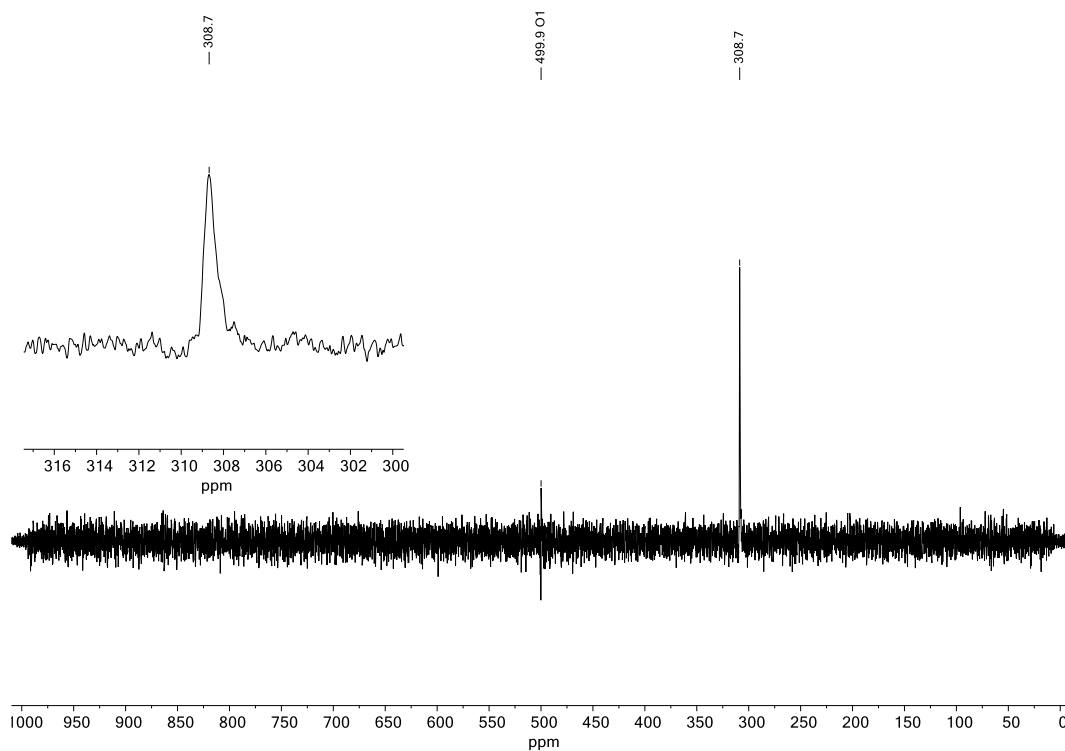


Figure S7. $^{35}\text{Cl}\{^1\text{H}\}$ NMR spectrum (49.0 MHz, *o*DFB/ C_6D_{12} 5:1) of $[\text{nBu}_4\text{N}][\mathbf{2}]$. The peak annotated with “O1” (offset frequency) is an artefact.

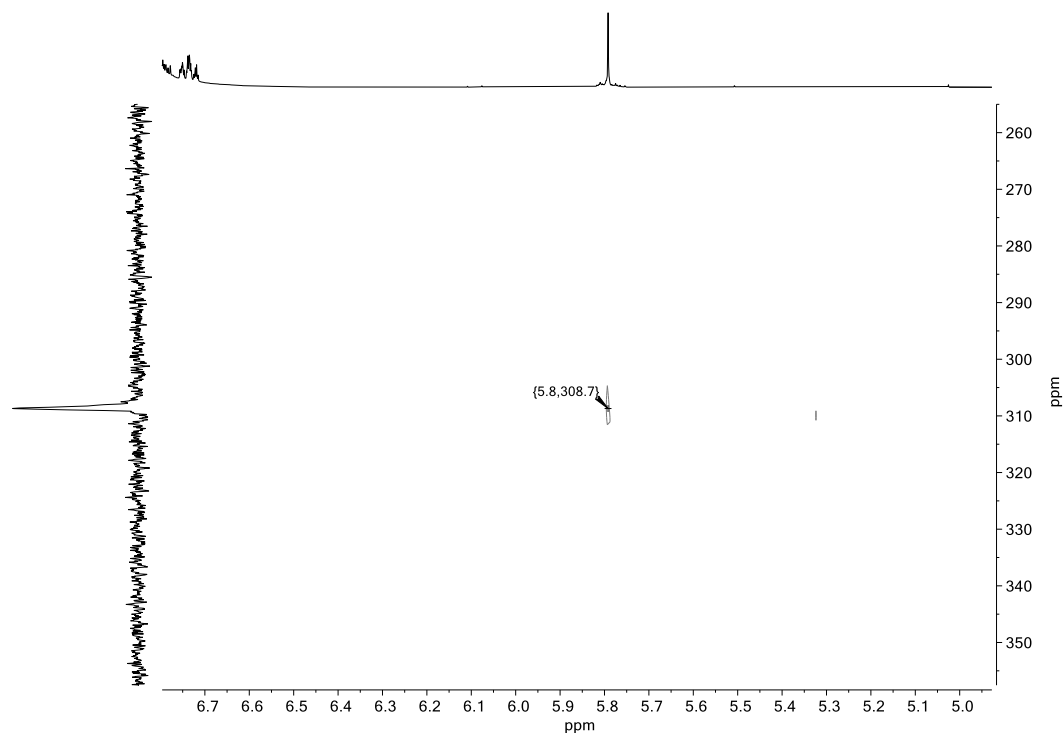


Figure S8. $^1\text{H}^{35}\text{Cl}$ -HMBC NMR spectrum (500.2 / 49.0 MHz, *o*DFB/ C_6D_{12} 5:1) of $[\text{nBu}_4\text{N}][\mathbf{2}]$.

3.2. NMR spectra of $[n\text{Bu}_4\text{N}][\mathbf{3}]$

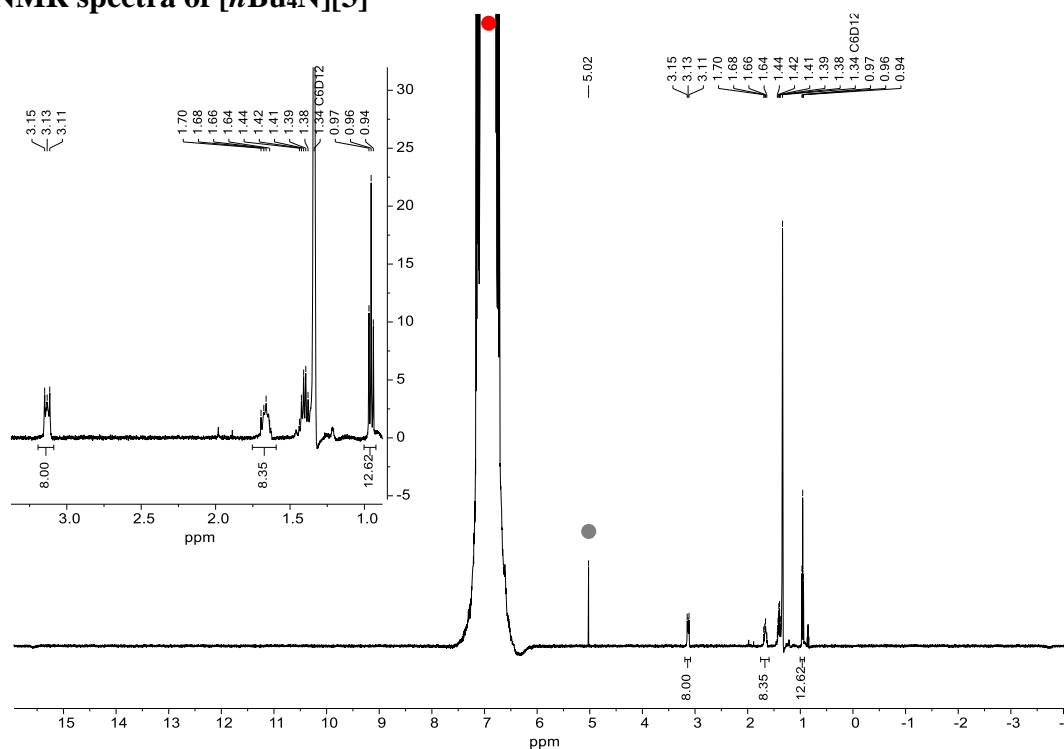


Figure S9. ^1H NMR spectrum (500.2 MHz, *o*DFB/ C_6D_{12} 5:1) of $[n\text{Bu}_4\text{N}][\mathbf{3}]$. The solvent signal of *o*DFB is marked with a red dot; the signal marked with a grey dot is due to an impurity from the *o*DFB.

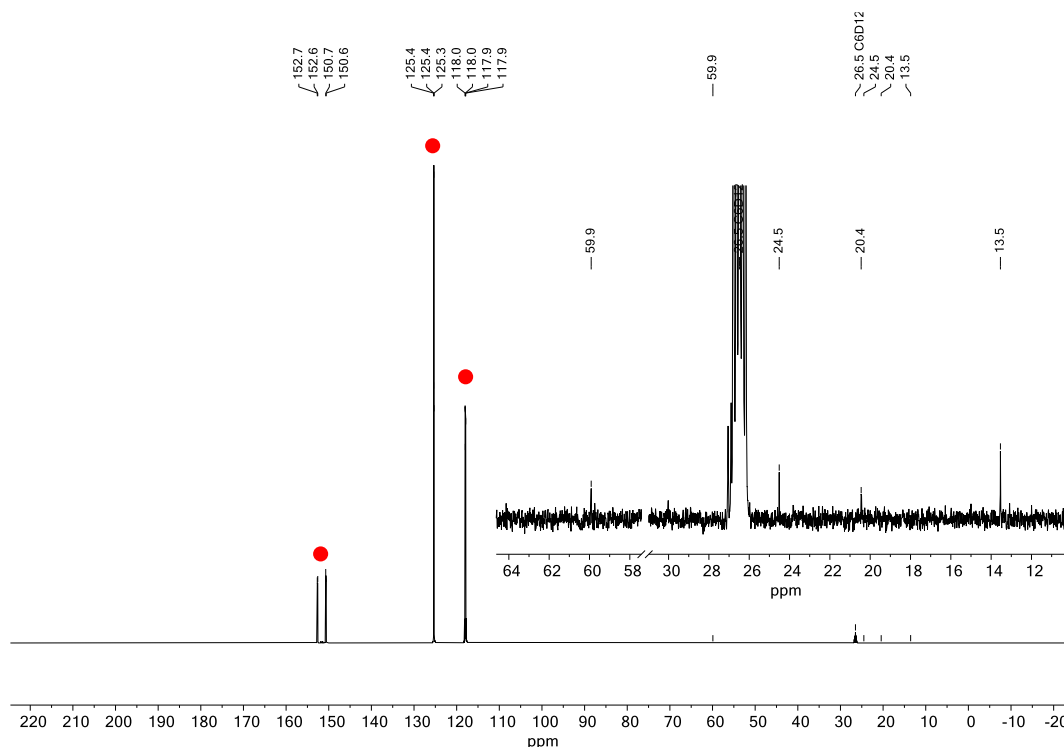


Figure S10. $^{13}\text{C}\{^1\text{H}\}$ NMR spectrum (125.8 MHz, *o*DFB/ C_6D_{12} 5:1) of $[n\text{Bu}_4\text{N}][\mathbf{3}]$. The solvent signals of *o*DFB are marked with red dots.

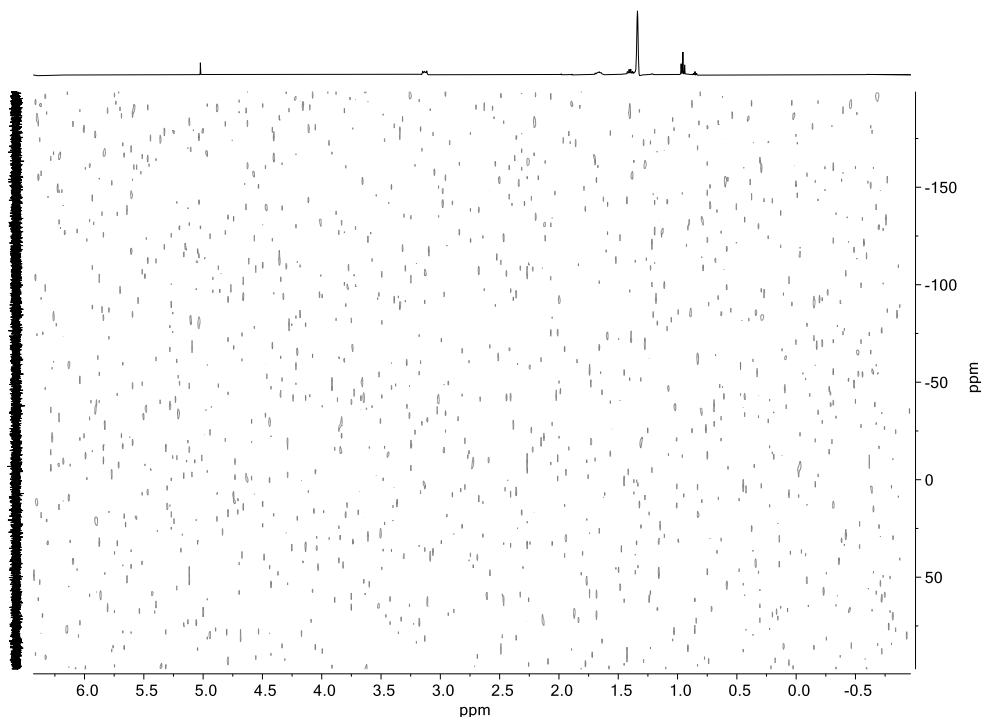


Figure S11. ^1H - ^{29}Si -HSQC NMR spectrum (500.2 / 99.4 MHz, *o*DFB/ C_6D_{12} 5:1) of $[\text{nBu}_4\text{N}][\mathbf{3}]$. No cross peak, which might indicate the presence of Si-bonded H atoms, was found.

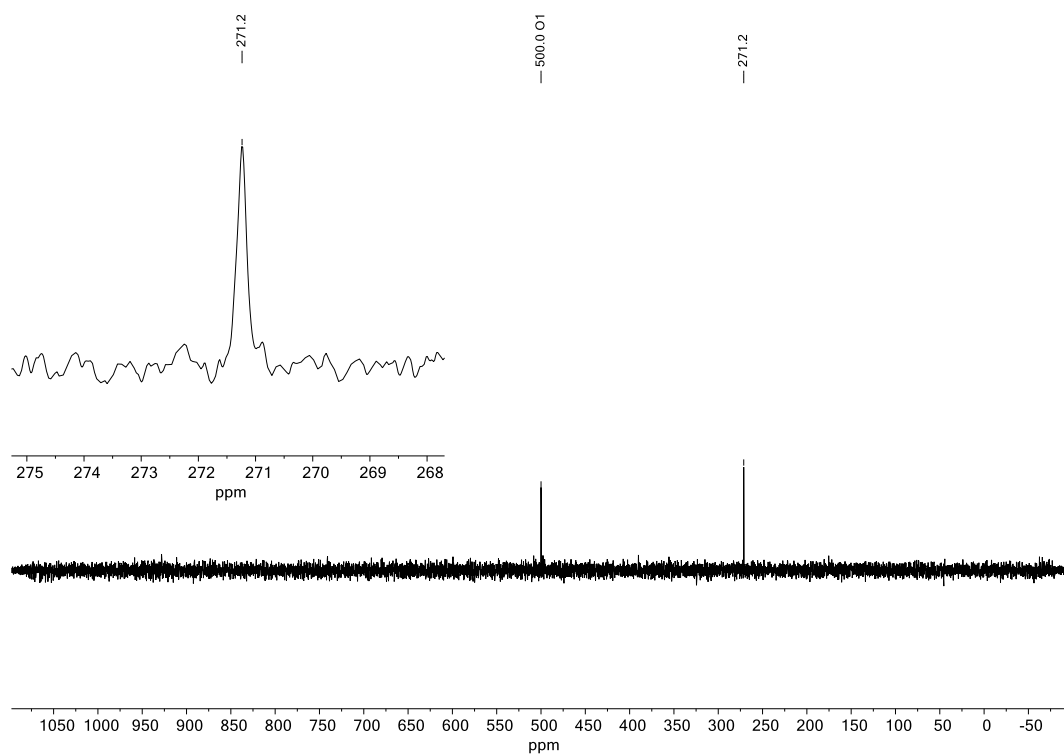


Figure S12. $^{35}\text{Cl}\{^1\text{H}\}$ NMR spectrum (49.0 MHz, *o*DFB/ C_6D_{12} 5:1) of $[\text{nBu}_4\text{N}][\mathbf{3}]$. The peak annotated with “O1” (offset frequency) is an artefact.

3.3. NMR spectra of $[n\text{Bu}_4\text{N}][\mathbf{4}]$

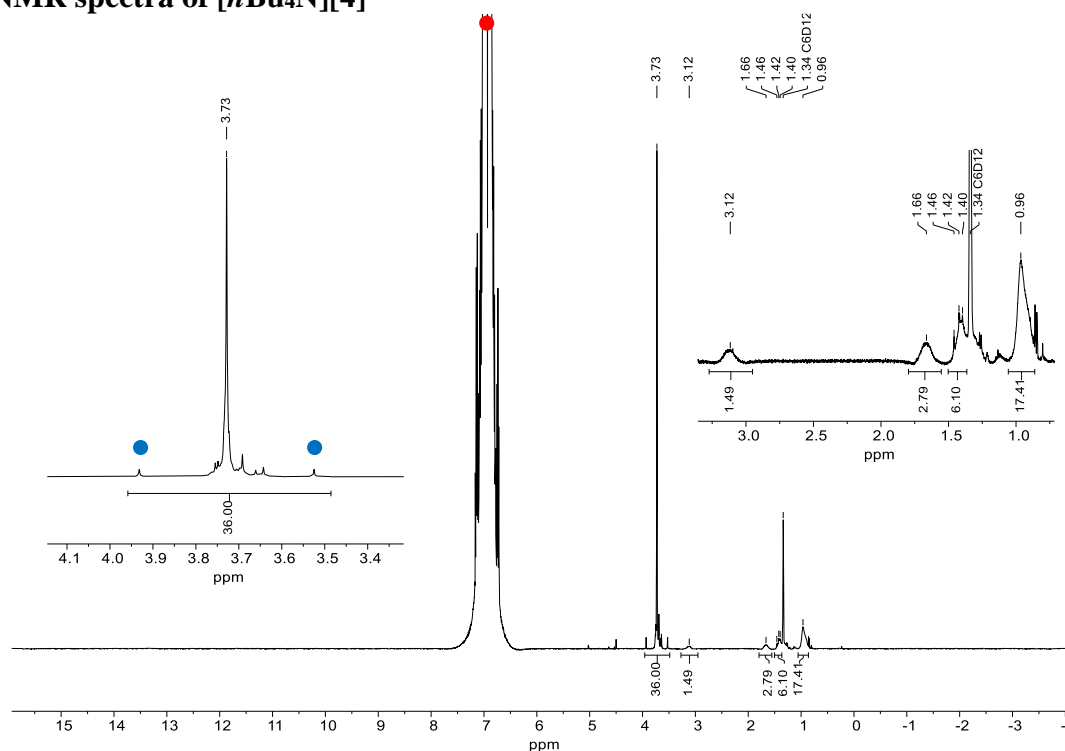


Figure S13. ^1H NMR spectrum (500.2 MHz, $o\text{DFB}/\text{C}_6\text{D}_{12}$ 5:1) of $[n\text{Bu}_4\text{N}][\mathbf{4}]$. ^{29}Si satellites are marked with blue dots, the solvent signal of $o\text{DFB}$ is marked with a red dot.

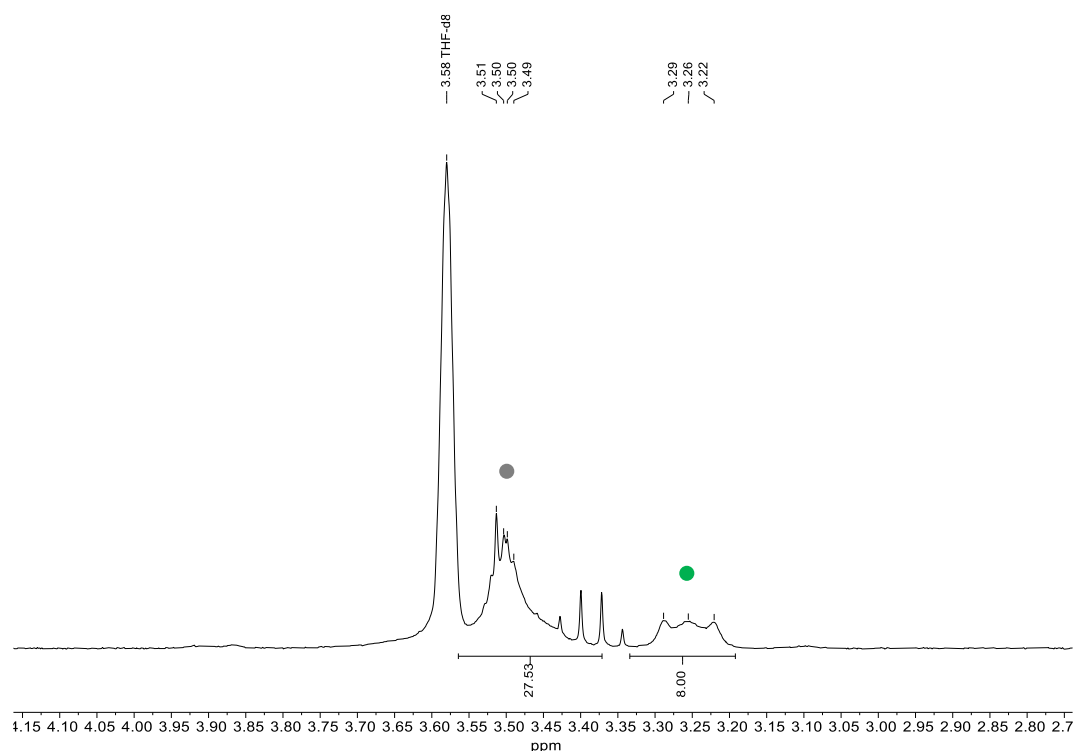


Figure S14. Characteristic region of the ^1H NMR spectrum (500.2 MHz, $\text{THF-}d_8$) of $[n\text{Bu}_4\text{N}][\mathbf{4}]$. The multiplet of the cation signal (green dot) is well resolved, but the signal of the silafullerane anion is split and broadened due to solvent-induced decomposition (grey dot; cf. the singlet at 3.73 ppm in Figure S13 for comparison).

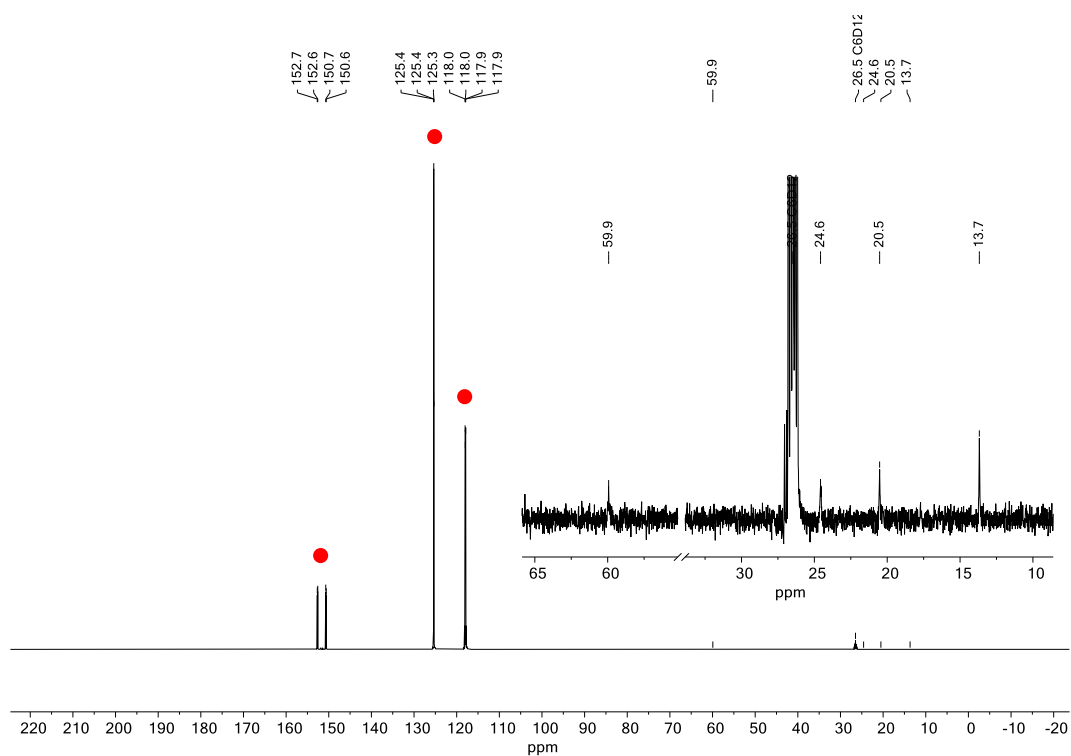


Figure S15. $^{13}\text{C}\{^1\text{H}\}$ NMR spectrum (125.8 MHz, *o*DFB/ C_6D_{12} 5:1) of $[\text{nBu}_4\text{N}][\mathbf{4}]$. The solvent signals of *o*DFB are marked with red dots.

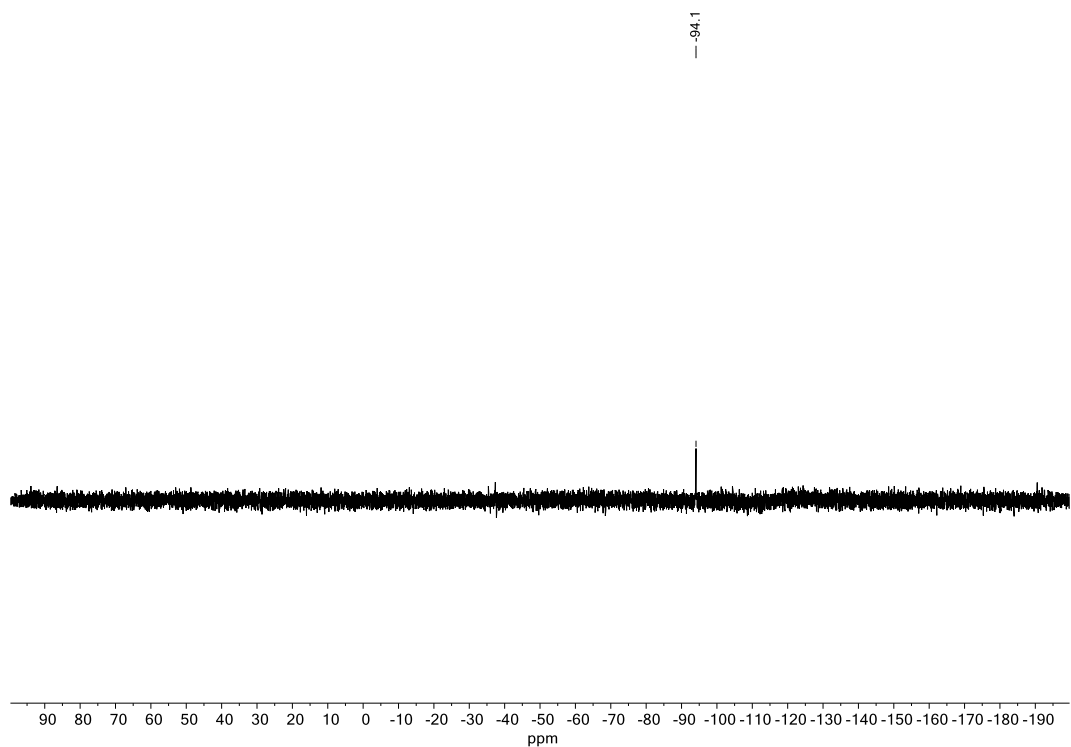


Figure S16. $^{29}\text{Si}\{^1\text{H}\}$ NMR spectrum (99.4 MHz, *o*DFB/ C_6D_{12} 5:1) of $[\text{nBu}_4\text{N}][\mathbf{4}]$.

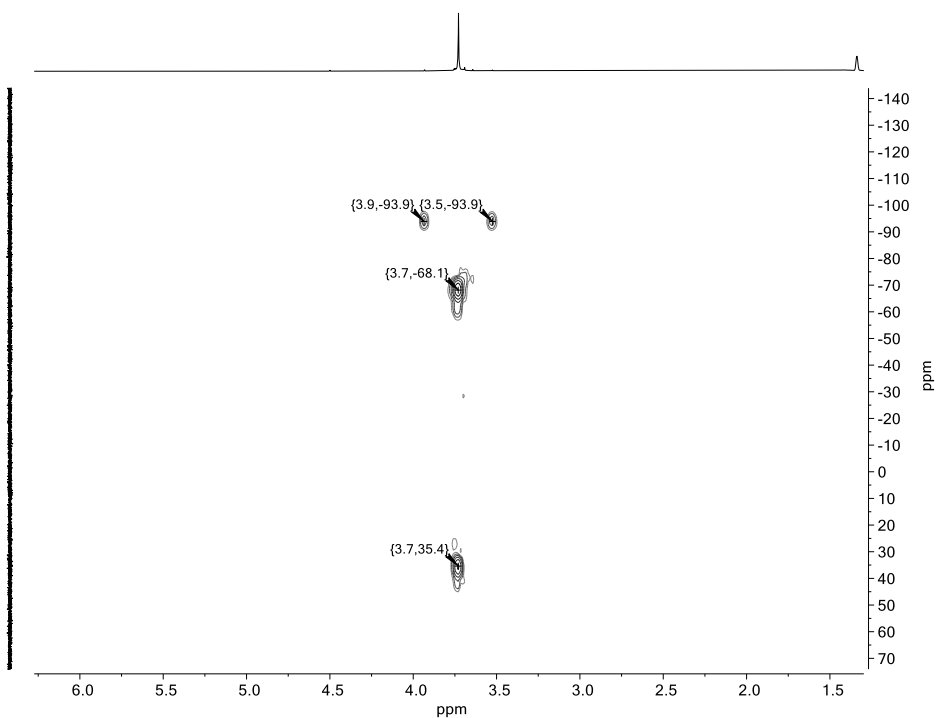


Figure S17. $^1\text{H}^{29}\text{Si}$ -HMBC NMR spectrum (500.2 / 99.4 MHz, *o*DFB/ C_6D_{12} 5:1) of $[\text{nBu}_4\text{N}][\mathbf{4}]$.

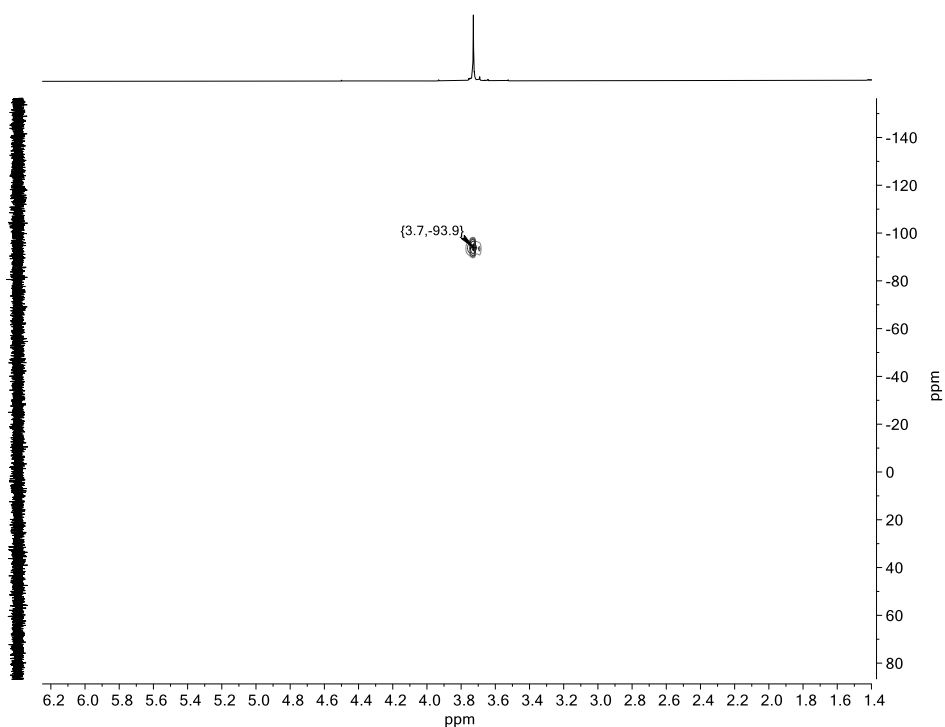


Figure S18. $^1\text{H}^{29}\text{Si}$ -HSQC NMR spectrum (500.2 / 99.4 MHz, *o*DFB/ C_6D_{12} 5:1) of $[\text{nBu}_4\text{N}][\mathbf{4}]$.

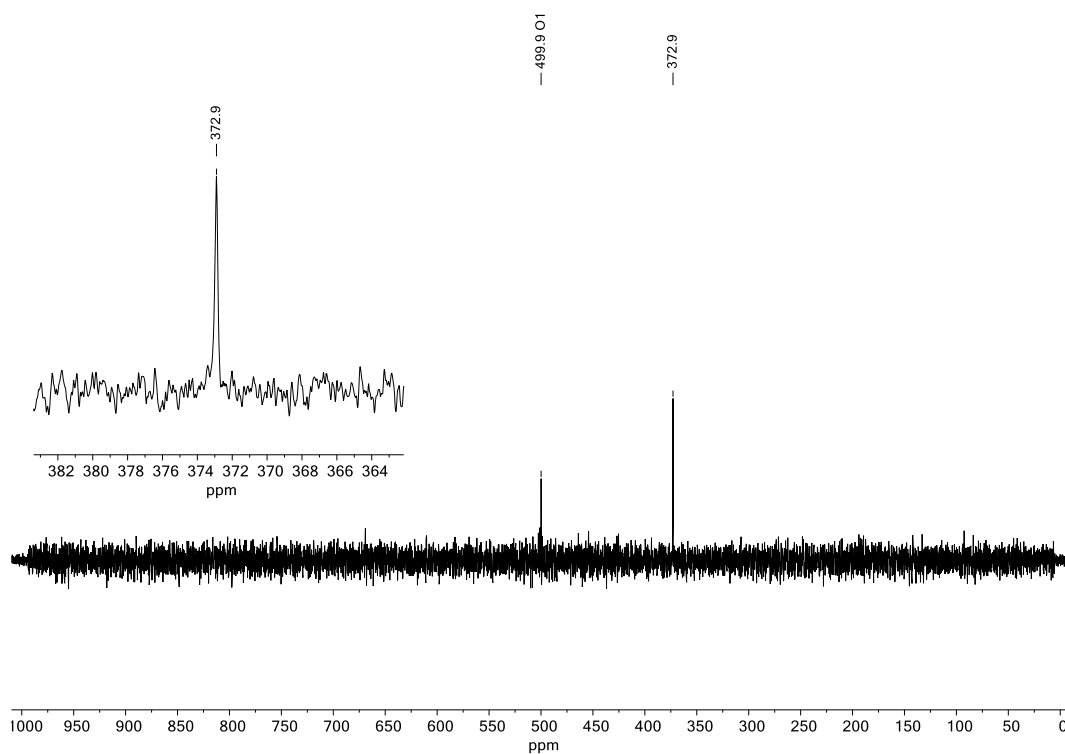


Figure S19. $^{35}\text{Cl}\{^1\text{H}\}$ NMR spectrum (49.0 MHz, *o*DFB/ C_6D_{12} 5:1) of $[\text{nBu}_4\text{N}][\mathbf{4}]$. The peak annotated with “O1” (offset frequency) is an artefact.

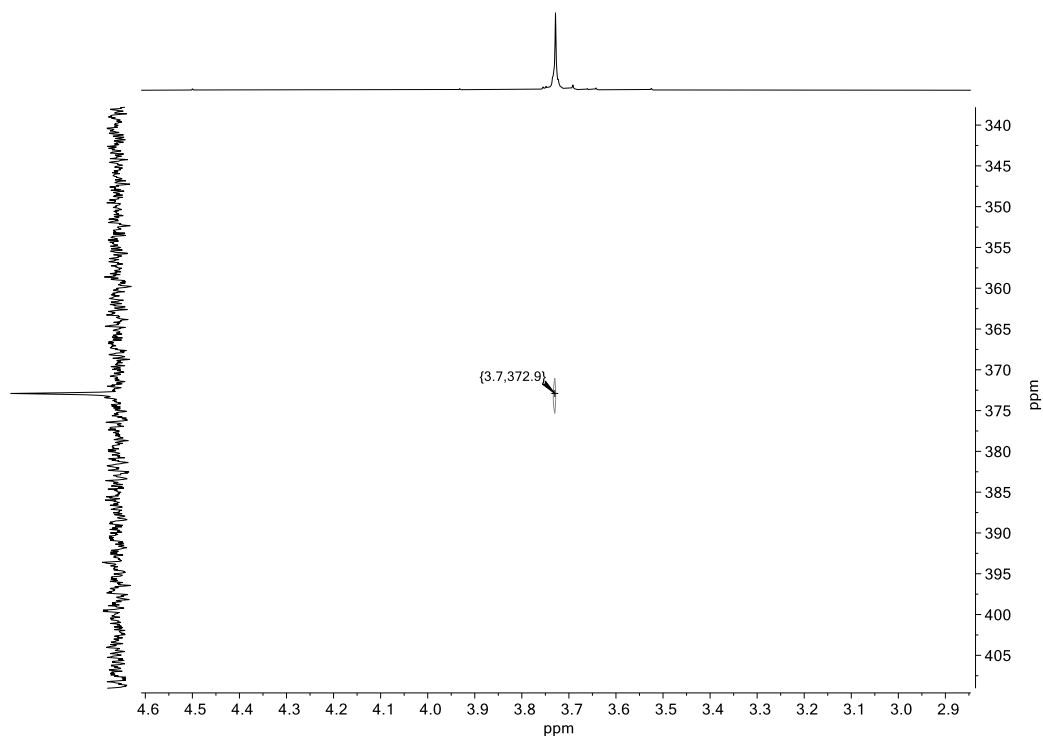


Figure S20. $^1\text{H}^{35}\text{Cl}$ -HMBC NMR spectrum (500.2 / 49.0 MHz, *o*DFB/ C_6D_{12} 5:1) of $[\text{nBu}_4\text{N}][\mathbf{4}]$.

4. Plots of mass spectra

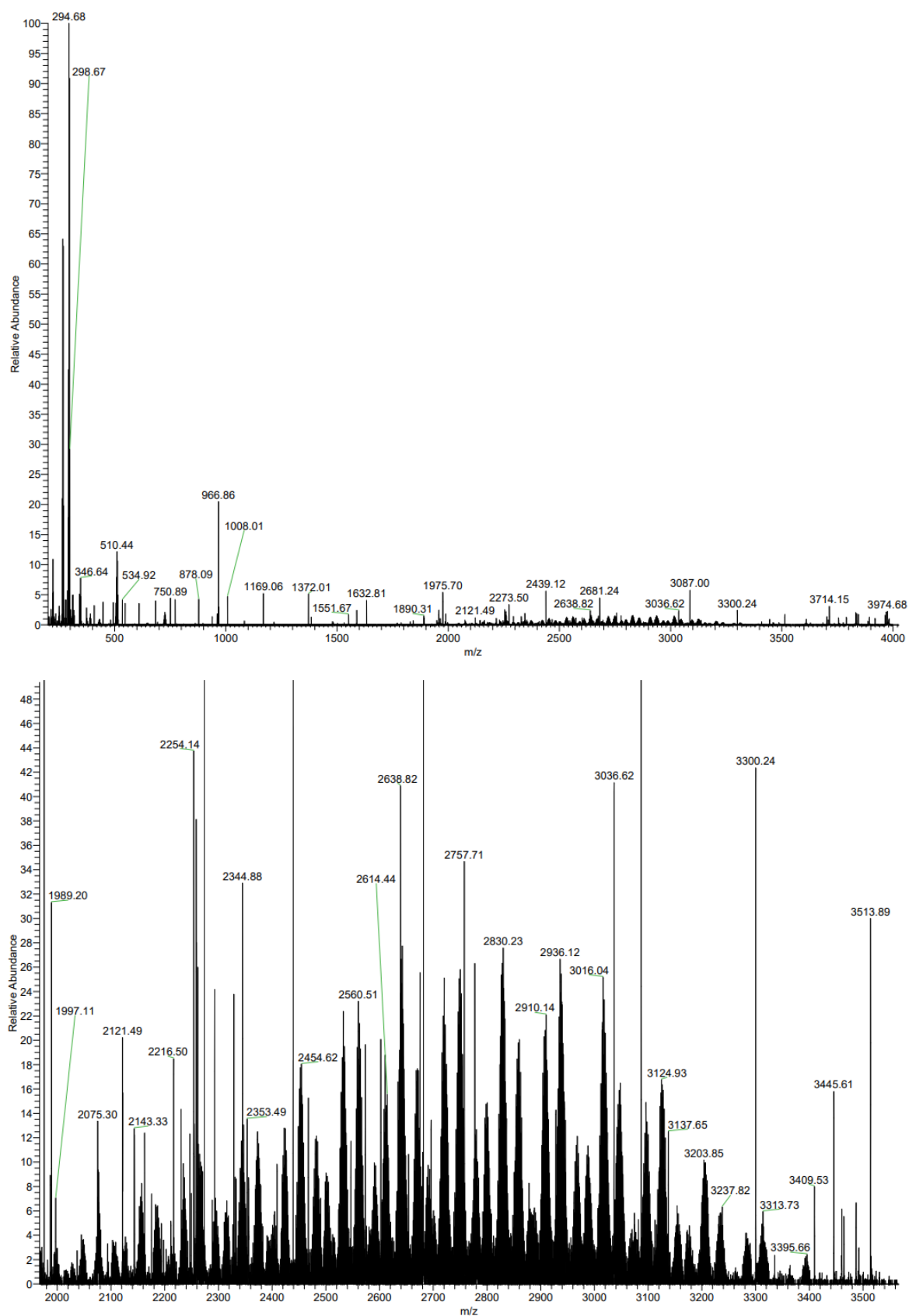


Figure S21. LDI(-) mass spectrum of $[n\text{Bu}_4\text{N}][2]$ (top: full spectrum; bottom: characteristic region).

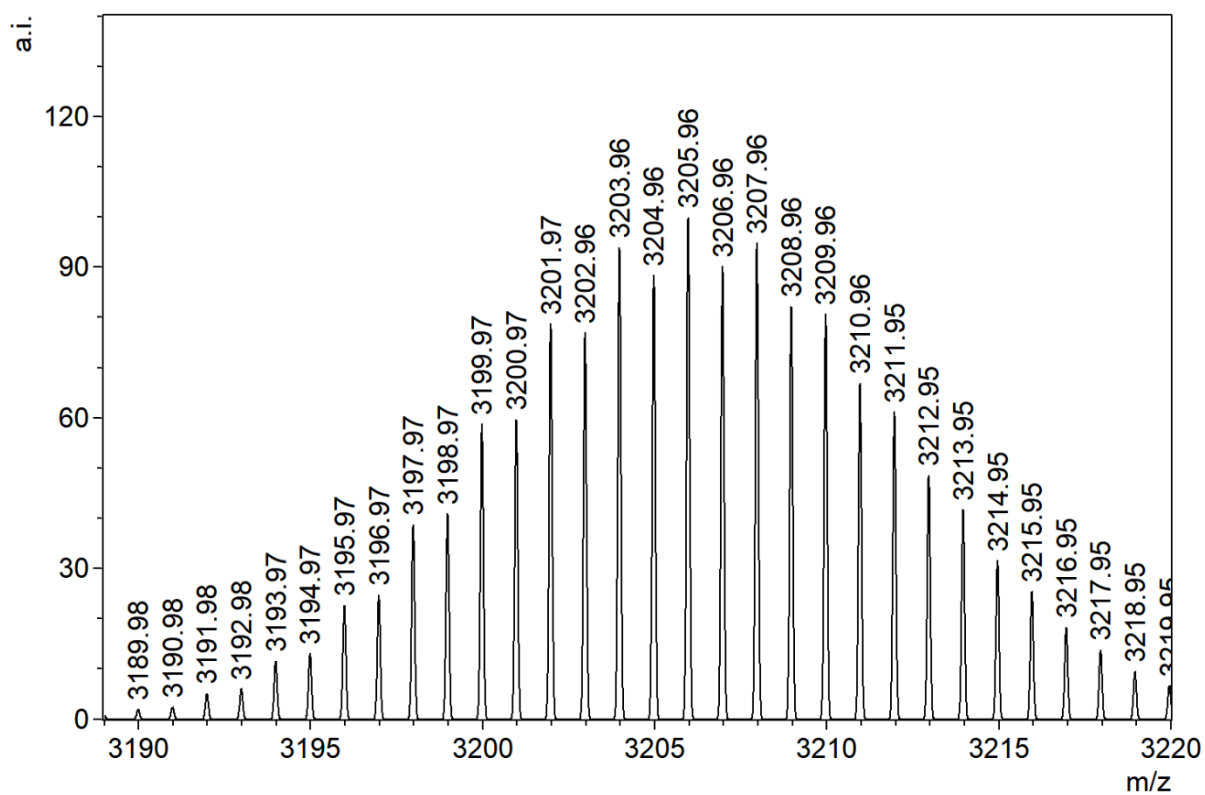
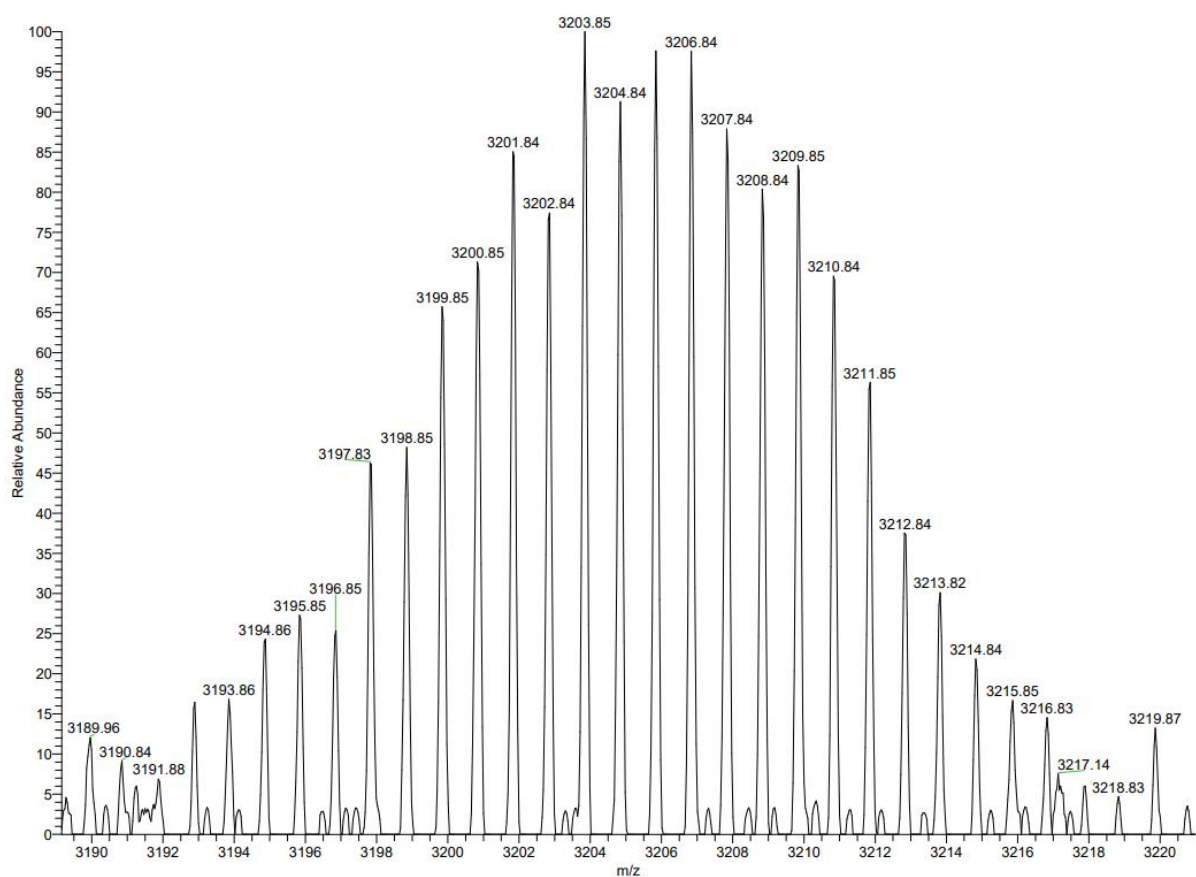


Figure S22. Measured (top; $[\text{nBu}_4\text{N}][\mathbf{2}]$) and simulated (bottom) isotope pattern of $[\text{Cl}@Si_{30}H_{11}Br_{29}]^-$, the largest fragmentation product of $[\mathbf{2}]^-$, the isotope pattern of which was well resolved.

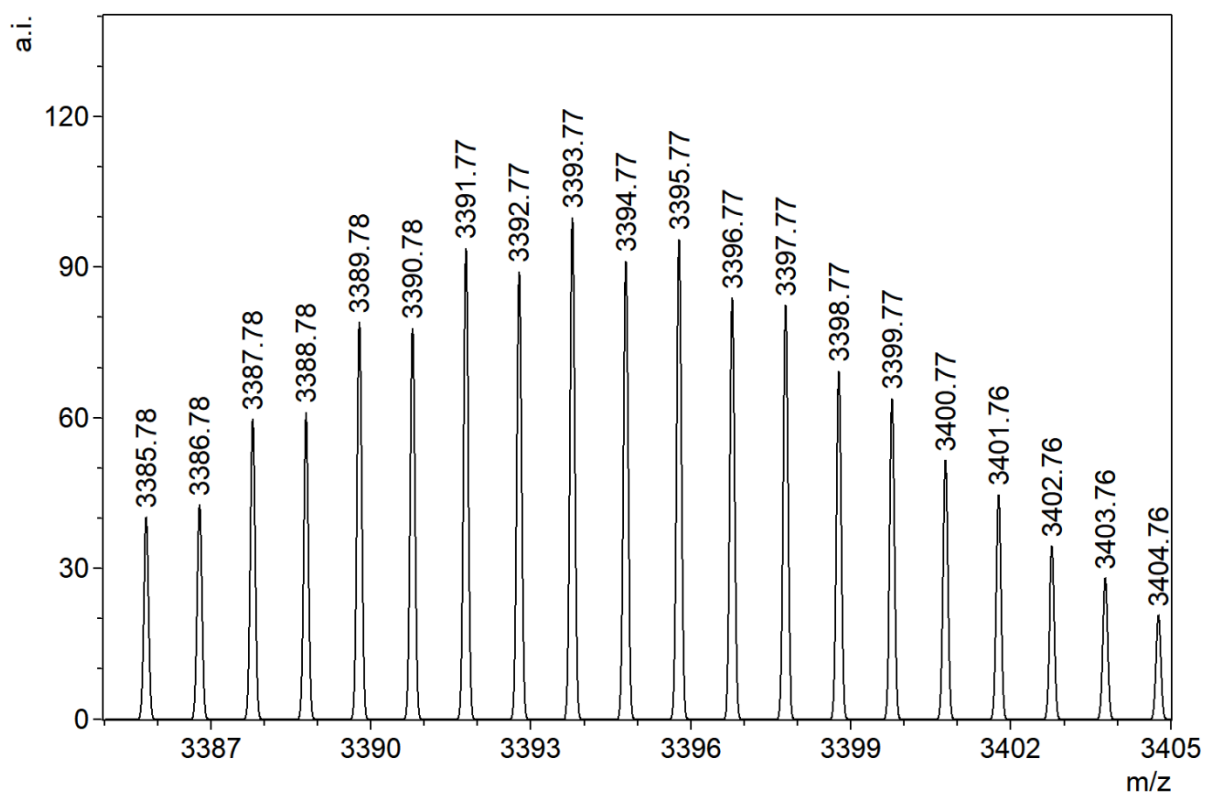
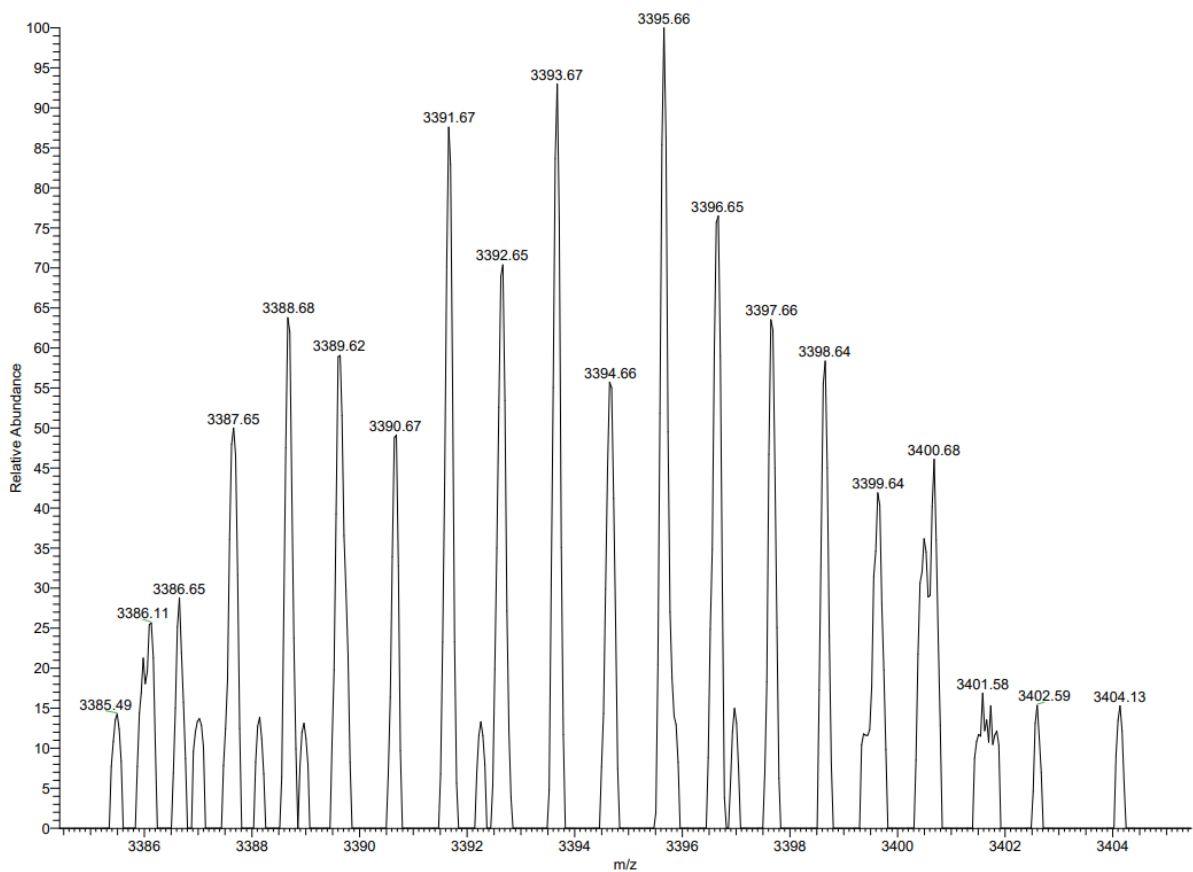


Figure S23. Measured (top) and simulated (bottom) isotope pattern of $[\text{Cl}@\text{Si}_{31}\text{H}_{11}\text{Br}_{31}]^-$, the largest fragmentation product detected in the LDI(-) mass spectrum of $[\text{nBu}_4\text{N}][\mathbf{2}]$.

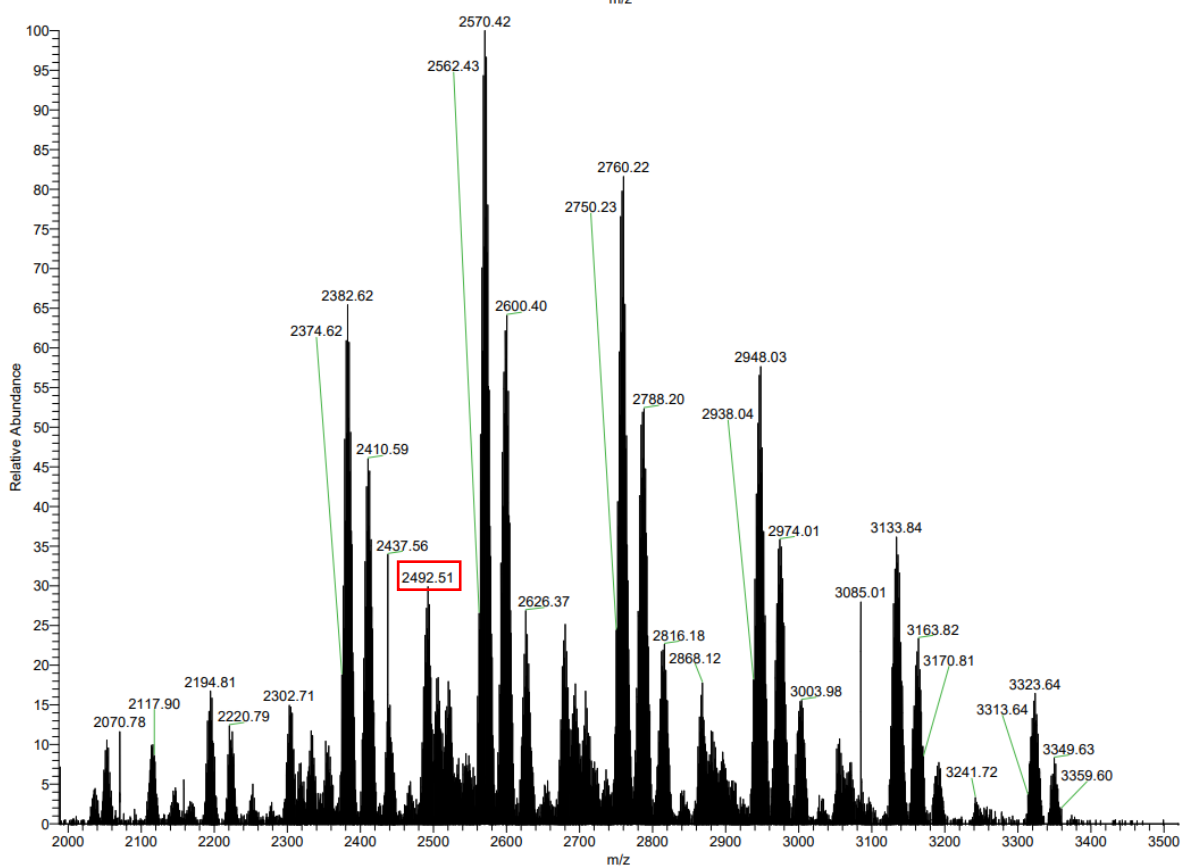
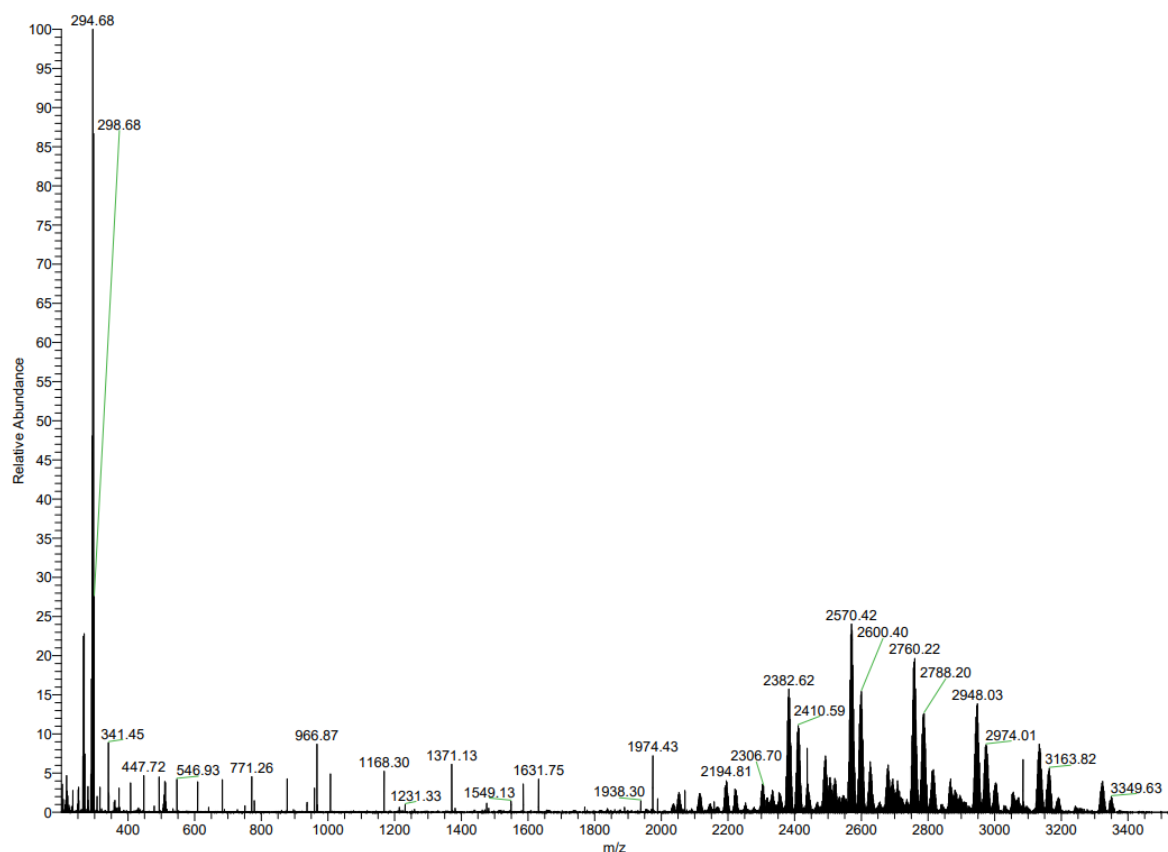


Figure S24. LDI(-) mass spectrum of $[n\text{Bu}_4\text{N}][\mathbf{3}]$ (top: full spectrum; bottom: characteristic region). The peak with the highest intensity assigned to an incompletely brominated fragment is marked with a red box.

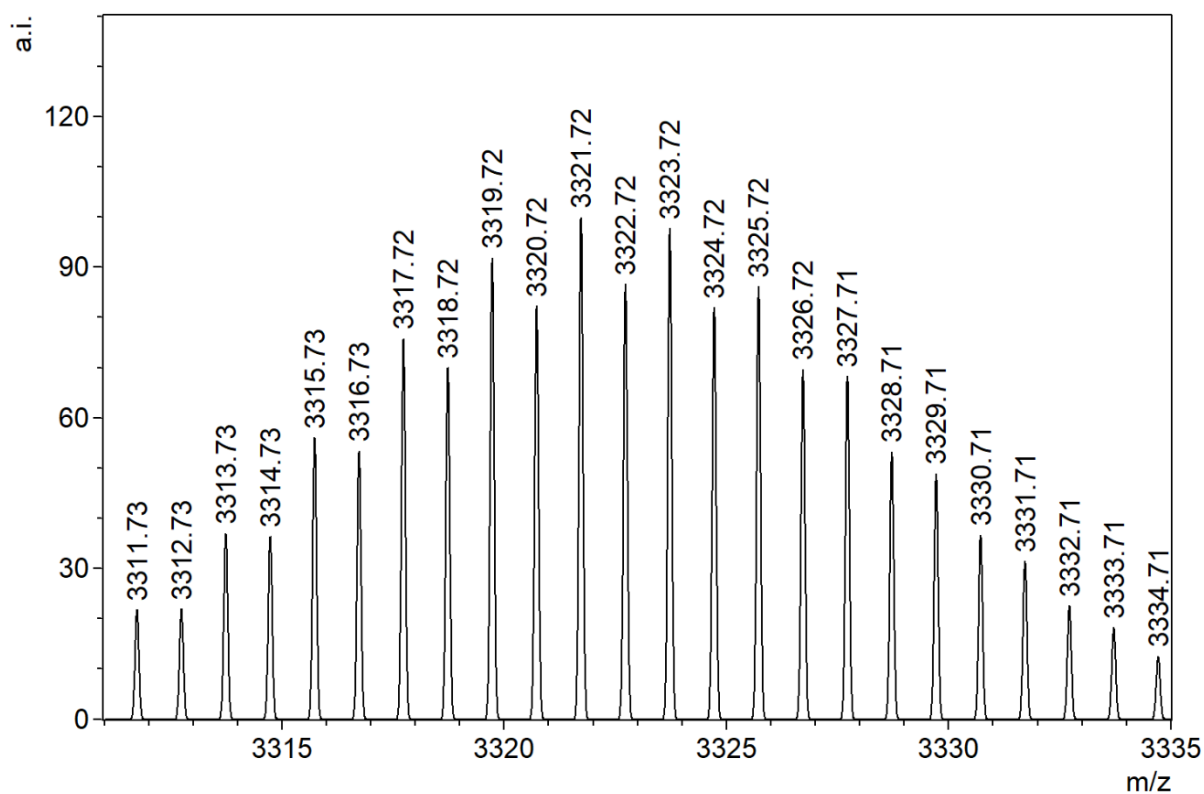
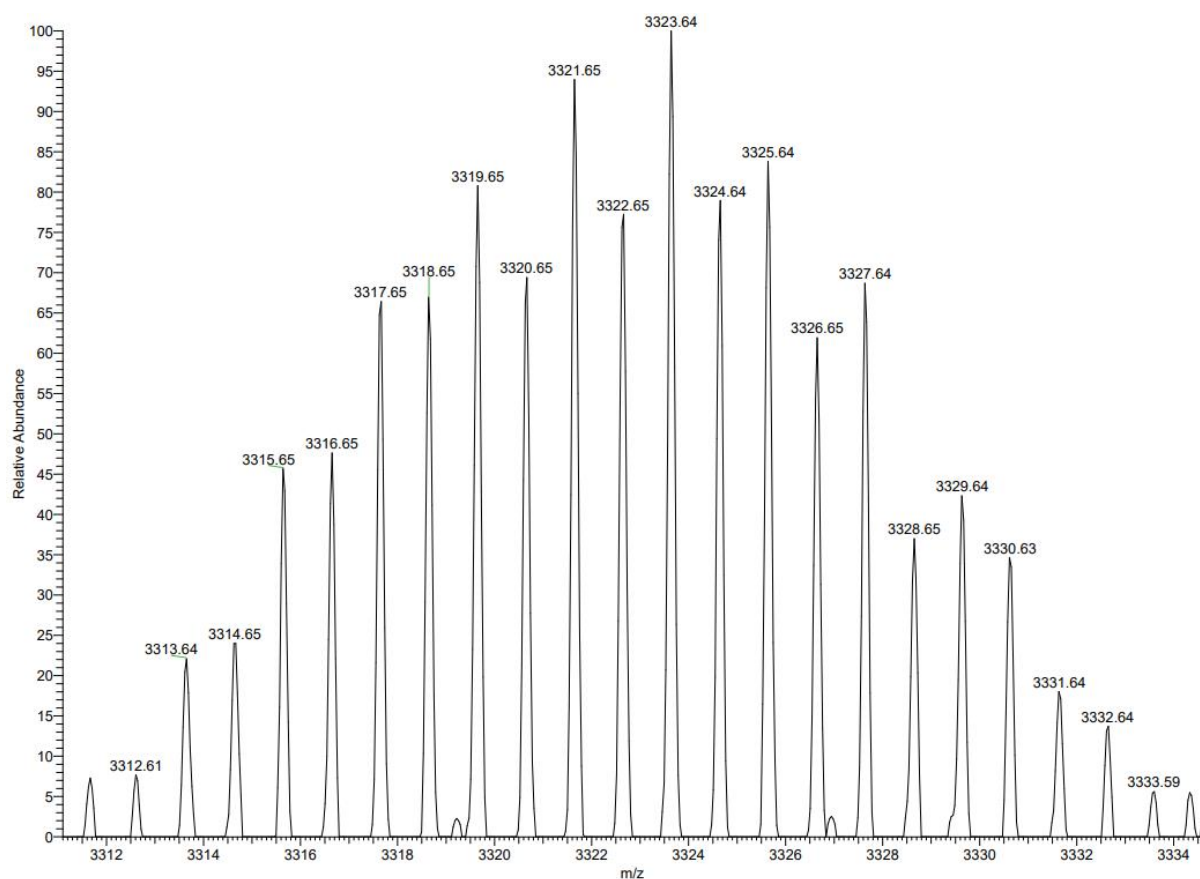


Figure S25. Measured (top; $[n\text{Bu}_4\text{N}][\mathbf{3}]$) and simulated (bottom) isotope pattern of $[\text{Cl}@\text{Si}_{26}\text{Br}_{32}]^-$, the largest fragmentation product of $[\mathbf{3}]^-$, the isotope pattern of which was well resolved.

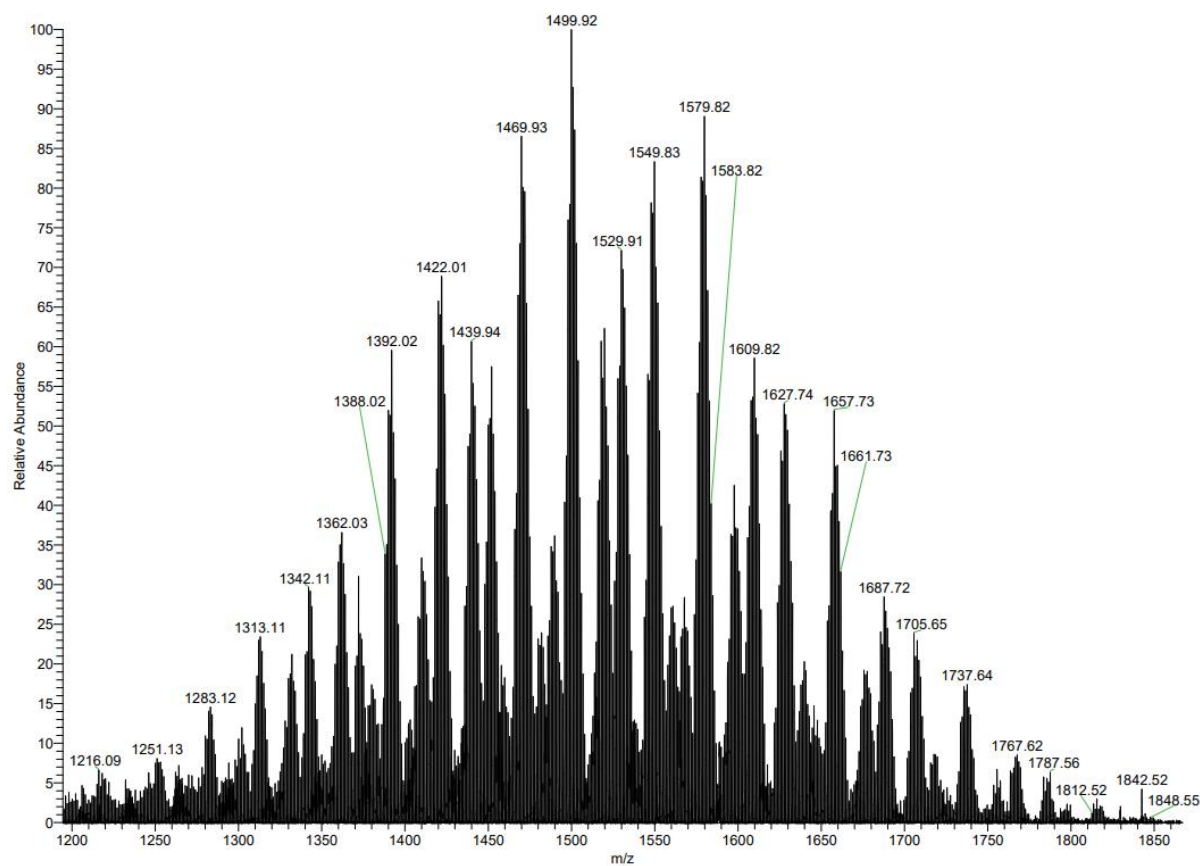
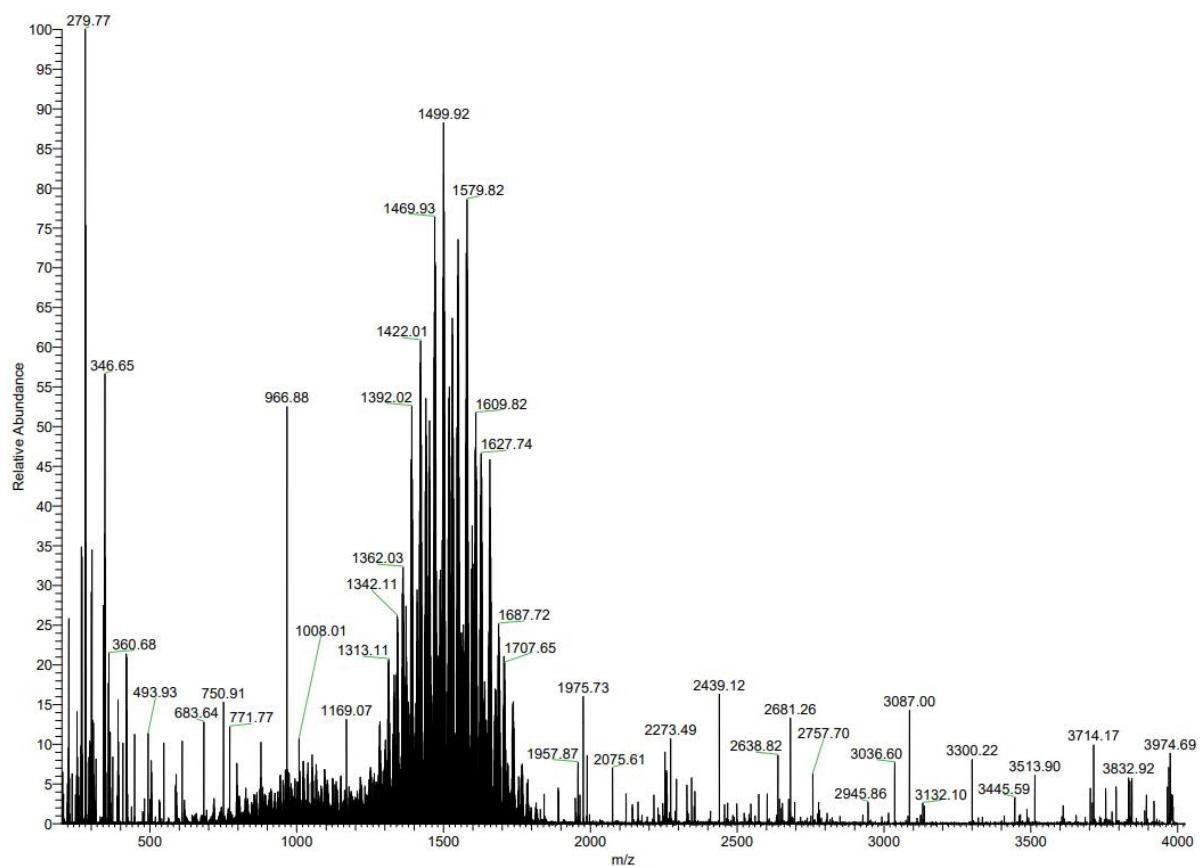


Figure S26. LDI(-) mass spectrum of [nBu₄N][4] (top: full spectrum; bottom: characteristic region).

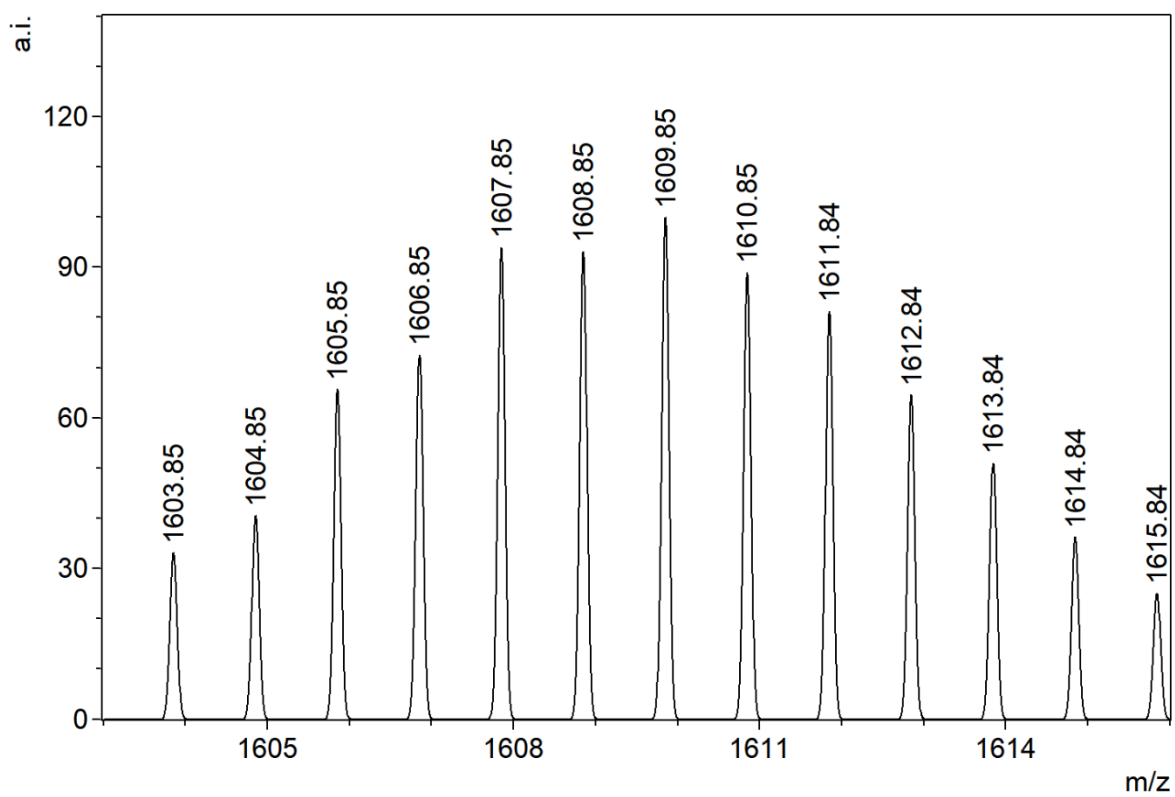
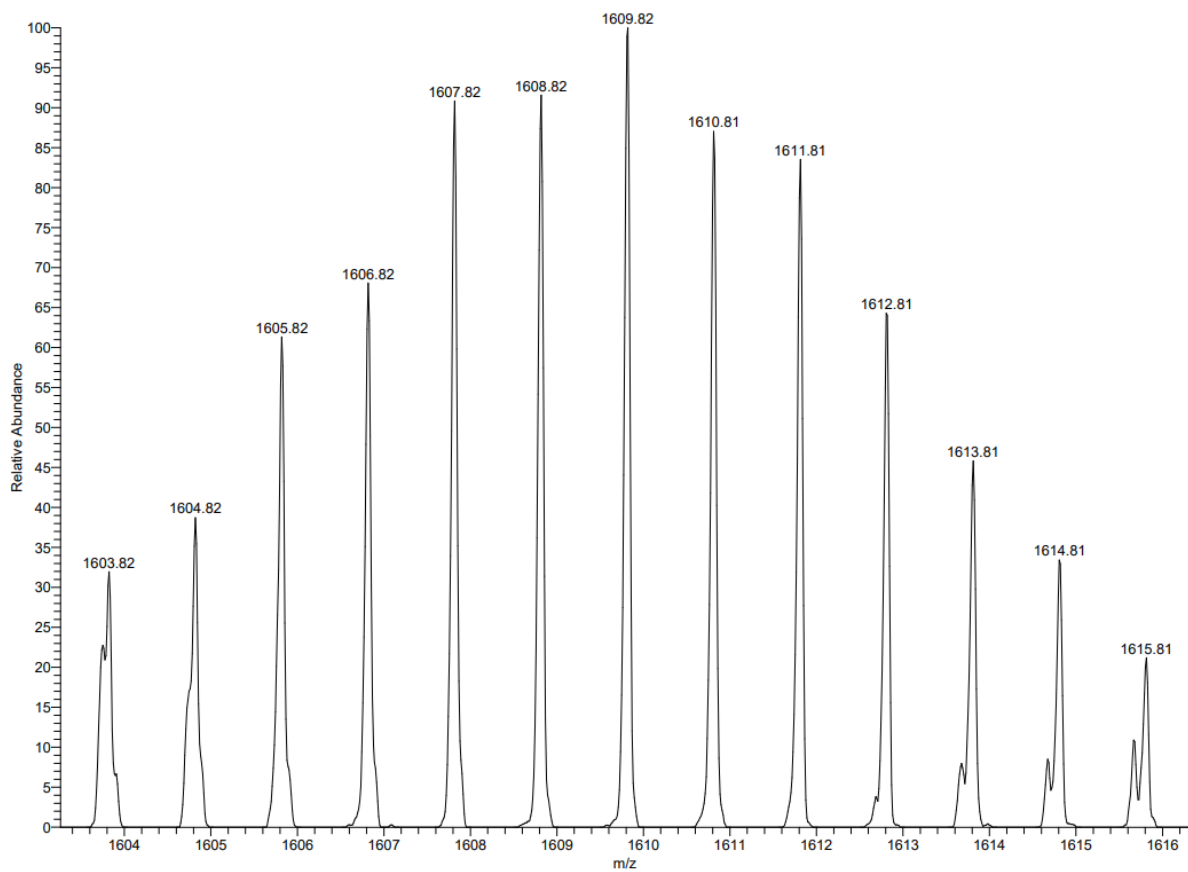


Figure S27. Measured (top; [nBu₄N][4]) and simulated (bottom) isotope pattern of [4]⁻.

5. X-ray crystal structure analyses

The diffraction data for [*n*Bu₄N][**2**] were collected at $T = 173(2)$ K on a *STOE IPDS II* two-circle diffractometer equipped with a high-flux *Xenocs Genix 3D HS Mo* microfocus X-ray source (MoK α radiation, $\lambda = 0.71073$ Å) and a 340 mm image plate detector. The diffraction data were measured by 1° ω -scans using the *STOE X-Area v.1.50* program set. The frames were imported into the *CrysAlisPro v.1.171.42.43a* program (Rigaku OD, 2022) using the *ESPERANTO Importer* tool for the subsequent indexing, integration, scaling, and the absorption correction. Due to the weak scattering ability of the single crystal of [*n*Bu₄N][**2**], all reflections above $d_{min} = 1.0$ Å were discarded. The structure was solved by direct methods using the *SHELXT* program^{S8} and refined in anisotropic approximation against $|F|^2$ using the *SHELXL-2018/3* program.^{S9} The positions of H atoms of the SiHBr₂ groups in [*n*Bu₄N][**2**] were set geometrically and refined in the rigid body approximation (AFIX 13). Because there are no reliable structural data on SiHBr₂ fragments, the Si–H distance was fixed at 1.326 Å. This value was taken from the structure of CH₃SiHCl₂ (CSD code DARJOY) that had been refined with $R_1 = 2.6\%$.^{S10}

The diffraction data for [*n*Bu₄N][**3**] were collected at the P24 beamline of the DESY PETRA III synchrotron^{S11} equipped with a four-circle *HUBER* diffractometer with Eulerian geometry and a *DECTRIS PILATUS3 CdTe 1M* pixel array detector at $T = 100(2)$ K using an open-flow nitrogen cryosystem. The data were acquired by 360° ϕ -rotation with 0.2° scan width and an exposure time of 1.2 s per frame at the wavelength $\lambda = 0.56002$ Å (22.139 keV). The frames were imported into the *CrysAlisPro v.1.171.42.43a* program (Rigaku OD, 2022) using the *ESPERANTO Importer* tool for the subsequent indexing, integration, scaling, and the absorption correction. The structure was solved by direct methods using the *SHELXT* program^{S8} and refined in anisotropic approximation against $|F|^2$ using the *SHELXL-2018/3* program.^{S9}

Topological aspects of the crystal packing were analyzed with the *TOPOS 4.0 Professional* program set.^{S12}

The crystallographic data, details of the diffraction experiments, and refinements are given in Tables S3 and S4. CIF files containing the crystallographic information were deposited in the Cambridge Crystallographic Data Centre under the deposition codes CCDC 2260148 ([*n*Bu₄N][**2**]) and CCDC 2260149 ([*n*Bu₄N][**3**]) and can be obtained free of charge via www.ccdc.cam.ac.uk/data_request/cif.

Compound $[n\text{Bu}_4\text{N}][\mathbf{2}]$:

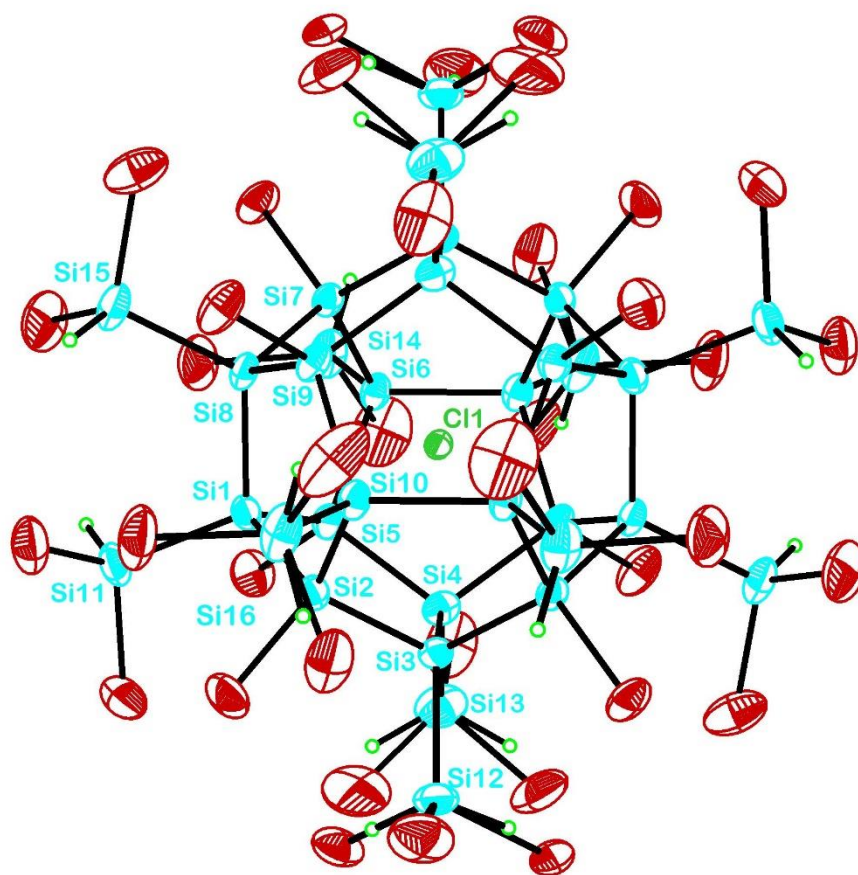


Figure S28. Molecular structure of $[n\text{Bu}_4\text{N}][\mathbf{2}]$ in the solid state. The $[n\text{Bu}_4\text{N}]^+$ cation is omitted for clarity; incompletely occupied Br and H positions are also depicted. Displacement ellipsoids are drawn at the 50% probability level. Ranges of atom \cdots atom distances [\AA], bond lengths [\AA], and angles [$^\circ$]: $\text{Cl}(1)\cdots\text{SiSiHBr}_2 = 3.312(3)\text{--}3.361(3)$, $\text{Cl}(1)\cdots\text{SiBr} = 3.230(3)\text{--}3.290(4)$, $\text{Si}^{\text{III}}\text{Br}\cdots\text{BrSi}^{\text{I}} = 3.791(3)\text{--}4.113(3)$, $\text{Si}^{\text{III}}\cdots\text{Si}^{\text{III}} = 4.260(6)\text{--}4.423(6)$, $\text{Si}^{\text{0}}\text{--SiHBr}_2 = 2.324(5)\text{--}2.339(5)$, $\text{Si}^{\text{0}}\text{--SiBr} = 2.341(5)\text{--}2.374(5)$, $\text{Si}^{\text{0}}\text{--Si}^{\text{0}} = 2.347(5)\text{--}2.364(5)$, $\text{Si}^{\text{I}}\text{--Br} = 2.233(3)\text{--}2.259(3)$, $\text{Si}^{\text{III}}\text{--Br} = 1.990(11)\text{--}2.220(4)$, $\text{Si}\text{--H} = 1.326$, $\text{Si}^{\text{III}}\text{--Si}^{\text{0}}\text{--Si}^{\text{0}} = 112.89(19)\text{--}118.30(18)$. Symmetry transformations used to generate equivalent atoms:

A: $-x+1, -y+1, -z+1$; B: $-x+3/2, -y+1/2, z$.

The $\{\text{Si}_{32}\}$ cage of $[\mathbf{2}]^-$ and its encapsulated Cl^- ion both lie on the same inversion center of the orthorhombic space group $Pccn$, while the $[n\text{Bu}_4\text{N}]^+$ cation occupies the position on the 2-fold axis. Three of the six crystallographically unique SiHBr_2 groups are orientationally disordered via rotation around Si–Si bonds. Two of them, $\text{Si}(4)\text{--Si}(13)\text{BrH}_2$ and $\text{Si}(10)\text{--Si}(16)\text{Br}_2\text{H}$, show two alternative orientations with relative weights of 80:20% and 90:10%, respectively. The

third one, Si(3)–Si(12)Br₂H, is disordered over all three positions with relative weights of 60:30:10%. The relative site occupancy factors (*sofs*) of the Br atoms were refined with fixed U_{iso} values. The sums of the *sofs* of the Br atoms were very close to 2 in all three cases, the value expected if only SiHBr₂ groups are present. At the next stage of the refinement, the *sof* variables were fixed at the refined values to avoid possible *sof-U* correlations. The final residual density map contained a couple of scattered peaks that might correspond to a severely disordered *o*DFB solvent molecule. Since all our attempts to describe these peaks failed, we applied the PLATON/SQUEEZE procedure.^{S13}

In the crystalline state, the [2]⁻ anions form a distorted body-centered tetragonal packing (<http://rcsr.net/nets/bct>), while the [*n*Bu₄N]⁺ cations are distributed according to a distorted hexagonal primitive net (<http://rcsr.net/nets/hex>). Their mutual spatial distribution cannot be classified as one of known 10,12-connected nets. The distances between the centroids are 13.86–15.00 Å and 13.86–16.84 Å for the cations and anions, respectively.

Compound $[n\text{Bu}_4\text{N}][\mathbf{3}]$:

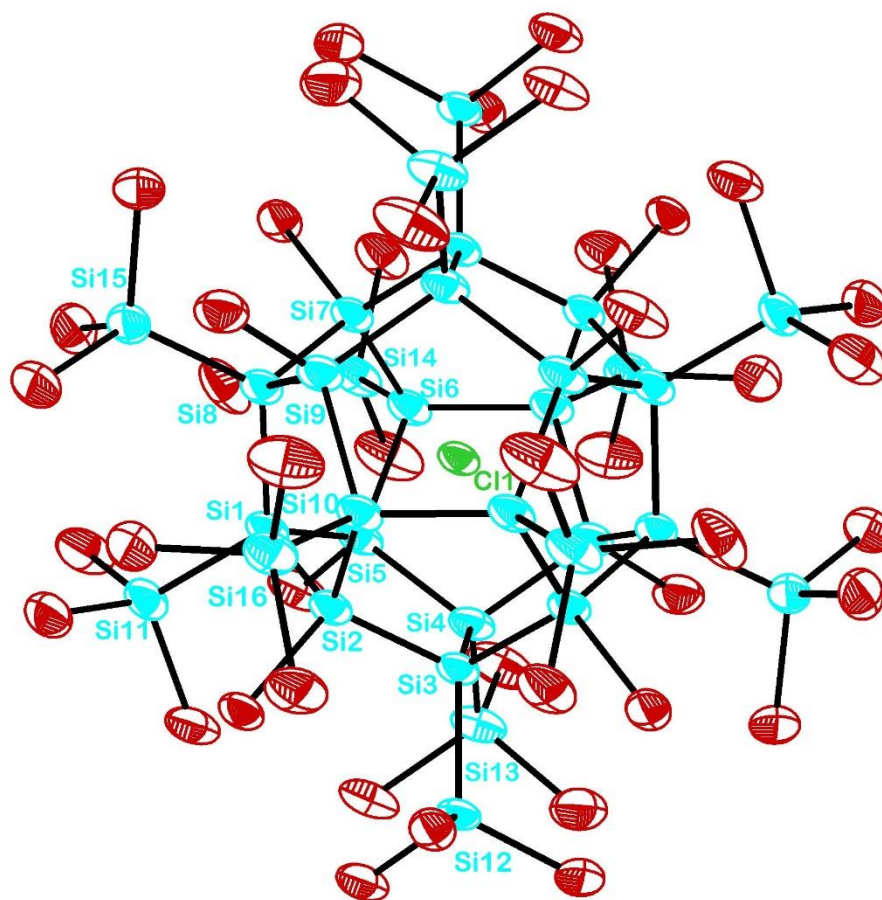


Figure S29. Molecular structure of $[n\text{Bu}_4\text{N}][\mathbf{3}]$ in the solid state. The $[n\text{Bu}_4\text{N}]^+$ cation is omitted for clarity. Displacement ellipsoids are drawn at the 50% probability level. Ranges of atom...atom distances [\AA], bond lengths [\AA], and angles [$^\circ$]: $\text{Cl}(1)\cdots\text{SiSiBr}_3 = 3.3373(17)\text{--}3.3486(14)$, $\text{Cl}(1)\cdots\text{SiBr} = 3.2653(17)\text{--}3.2965(19)$, $\text{Si}^{\text{III}}\text{Br}\cdots\text{BrSi}^{\text{III}} = 3.7022(12)\text{--}3.7823(15)$, $\text{Si}^{\text{III}}\text{Br}\cdots\text{BrSi}^{\text{I}} = 3.5866(11)\text{--}3.933(1)$, $\text{Si}^{\text{III}}\cdots\text{Si}^{\text{III}} = 4.578(3)\text{--}4.617(3)$, $\text{Si}^{\text{I}}\text{--SiBr}_3 = 2.329(2)\text{--}2.349(3)$, $\text{Si}^{\text{I}}\text{--SiBr} = 2.359(2)\text{--}2.376(2)$, $\text{Si}^{\text{I}}\text{--Si}^{\text{I}} = 2.360(2)\text{--}2.369(2)$, $\text{Si}^{\text{I}}\text{--Br} = 2.2270(16)\text{--}2.2365(16)$, $\text{Si}^{\text{III}}\text{--Br} = 2.1709(19)\text{--}2.231(2)$, $\text{Si}^{\text{III}}\text{--Si}^{\text{I}}\text{--Si}^{\text{I}} = 116.31(9)\text{--}120.39(8)$. Symmetry transformations used to generate equivalent atoms: A: $-x+1, -y+1, -z+1$; B: $-x, y, -z+3/2$.

The $\{\text{Si}_{32}\}$ cage of $[\mathbf{3}]^-$ and its encapsulated Cl^- ion both lie on the same inversion center of the monoclinic space group $C2/c$, while the $[n\text{Bu}_4\text{N}]^+$ cation occupies the position on the 2-fold axis, ensuring the charge balance. Two of the four $n\text{Bu}$ chains are statistically disordered over two positions with relative weights of 60:40%. Analysis of the atomic displacement parameters of the Br atoms as well as an independent refinement of their site-occupancy factors prove that

all terminal silyl groups are fully brominated (SiBr_3). The final residual density map contained a group of scattered peaks that might correspond to a severely disordered organic molecule. It might be an *o*DFB solvent molecule; however, even high-quality diffraction data from the synchrotron did not allow for an unambiguous interpretation, most probably due to the low contribution of light atoms to scattering that is mostly determined by the heavy $\{\text{Si}_{32}\text{Br}_{44}\}$ core. Therefore, we applied the PLATON/SQUEEZE procedure.^{S13}

In contrast to the crystal structure of $[\text{nBu}_4\text{N}][\mathbf{2}]$, the $[\mathbf{3}]^-$ anions form a rather unexpected, distorted primitive hexagonal packing (<http://rcsr.net/nets/hex>), while the $[\text{nBu}_4\text{N}]^+$ cations are distributed according to a significantly distorted hexagonal closest packing (<http://rcsr.net/nets/hcp>). Their mutual spatial distribution cannot be classified as one of known 12,12-connected nets. The distances between the centroids here are significantly larger, 15.38–17.71 Å and 14.50–15.35 Å for the cations and anions, respectively.

Table S3. Selected crystallographic data for [nBu₄N][2].

	[nBu ₄ N][2]
CCDC	2260148
Crystal data	
Chemical formula	C ₁₆ H ₄₈ Br ₃₂ CINSi ₃₂
<i>M</i> _r	3746.00
Crystal system	orthorhombic
Space group	<i>Pccn</i>
<i>T</i> (K)	173(2)
<i>a</i> (Å)	13.8596(8)
<i>b</i> (Å)	26.5550(17)
<i>c</i> (Å)	29.2504(16)
<i>α</i> (°)	90
<i>β</i> (°)	90
<i>γ</i> (°)	90
<i>V</i> (Å ³)	10765.4(11)
<i>Z</i>	4
<i>F</i> (000)	6944
<i>D</i> _{calcd} (g cm ⁻³)	2.311
Radiation, <i>λ</i> (Å)	MoK _α , 0.71073
<i>μ</i> (mm ⁻¹)	12.292
Crystal shape	plate
Color	colorless
Crystal size (mm)	0.16 × 0.15 × 0.04
Data collection	
Diffractometer	STOE IPDS II diffractometer, STOE image plate (340 mm diameter)
Radiation source	Xenocs Genix 3D HS Mo microfocus X-ray source
Absorption correction	Multi-scan, <i>CrysAlis PRO</i> 1.171.42.43a (Rigaku Oxford Diffraction, 2022), empirical absorption correction using spherical harmonics, implemented in <i>SCALE3 ABSPACK</i> scaling algorithm.
<i>T</i> _{min} , <i>T</i> _{max}	0.244, 0.639
No. of measured, independent, and observed [<i>I</i> > 2σ(<i>I</i>)] reflections	71223, 5612, 2884
<i>R</i> _{int}	0.1541
θ values (°)	θ _{max} = 20.8, θ _{min} = 3.8
Range of <i>h</i> , <i>k</i> , <i>l</i>	<i>h</i> = -13→13, <i>k</i> = -26→26, <i>l</i> = -27→29
Refinement	
<i>R</i> [<i>F</i> ² > 2σ(<i>F</i> ²)], <i>wR</i> (<i>F</i> ²), <i>S</i>	0.0396, 0.0870, 0.724
No. of reflections	5612
No. of parameters	401
No. of restraints	0
H-atom treatment	H-atom parameters constrained
Δρ _{max} , Δρ _{min} (e Å ⁻³)	2.151, -0.629

Table S4. Selected crystallographic data for [nBu₄N][3].

	[nBu ₄ N][3]
CCDC	2260149
Crystal data	
Chemical formula	C ₁₆ H ₃₆ Br ₄₄ CINSi ₃₂
<i>M_r</i>	4692.83
Crystal system	monoclinic
Space group	<i>C2/c</i>
<i>T</i> (K)	100(2)
<i>a</i> (Å)	15.2828(3)
<i>b</i> (Å)	26.6284(6)
<i>c</i> (Å)	29.0070(11)
<i>α</i> (°)	90
<i>β</i> (°)	91.721(2)
<i>γ</i> (°)	90
<i>V</i> (Å ³)	11799.2(6)
<i>Z</i>	4
<i>F</i> (000)	8576
<i>D</i> _{calcd} (g cm ⁻³)	2.642
Radiation, <i>λ</i> (Å)	synchrotron, 0.56002
<i>μ</i> (mm ⁻¹)	8.148
Crystal shape	elongated prism
Color	colorless
Crystal size (mm)	0.20 × 0.04 × 0.02
Data collection	
Diffractometer	DESY PETRA III P24 beamline, Huber diffractometer, Pilatus3 CdTe 1M detector
Radiation source	synchrotron
Absorption correction	Multi-scan, <i>CrysAlis PRO</i> 1.171.42.43a (Rigaku Oxford Diffraction, 2022), empirical absorption correction using spherical harmonics, implemented in SCALE3 ABSPACK scaling algorithm.
<i>T</i> _{min} , <i>T</i> _{max}	0.683, 1.000
No. of measured, independent, and observed [<i>I</i> > 2σ(<i>I</i>)] reflections	63706, 15465, 11809
<i>R</i> _{int}	0.0526
θ values (°)	θ _{max} = 24.1, θ _{min} = 2.1
Range of <i>h</i> , <i>k</i> , <i>l</i>	<i>h</i> = -22→21, <i>k</i> = -38→36, <i>l</i> = -39→35
Refinement	
<i>R</i> [<i>F</i> ² > 2σ(<i>F</i> ²)], <i>wR</i> (<i>F</i> ²), <i>S</i>	0.0576, 0.1642, 1.095
No. of reflections	15465
No. of parameters	445
No. of restraints	30
H-atom treatment	H-atom parameters constrained
Δρ _{max} , Δρ _{min} (e Å ⁻³)	1.980, -1.649

6. Computational details

6.1. General remarks and geometry optimizations

Quantum chemical calculations were performed with the AMS2022.101^{S14} (ADF module) and ORCA 5.0.3^{S15-17} program packages. Geometries were optimized with the hybrid composite-DFT method PBEh-3c^{S18-21} in conjunction with the universal continuum solvation model based on density (SMD)^{S22} for CH₂Cl₂ in ORCA. Minimum structures were verified by the absence of imaginary frequencies in a subsequent harmonic vibrational frequency calculation. Calculated frequencies were scaled with an empirical factor of 0.95 which is specific for PBEh-3c. In the optimization of [1]⁻ and [3]⁻, the resolution of identity approximation for Coulomb and Hartree-Fock (HF) Exchange integrals (RI-JK) has been applied with the respective auxiliary basis sets (def2/JK).^{S23} For all remaining calculations in ORCA the numerical chain-of-spheres integration for the HF Exchange integrals (RIJCOSX) with the matching auxiliary basis sets (def2/J)^{S24} has been applied instead.

6.2. Calculation of NMR shifts

All NMR shielding constants (σ) were calculated using gauge invariant atomic orbitals (GIAOs)^{S25} and the COSMO^{S26,27} implicit solvation model for CH₂Cl₂ (*surf Esurf, solv Eps=8.93 Rad =2.94, div ndiv=5* settings) in ADF of the AMS program package. Calculations were done with the zeroth order regular approximation (ZORA)^{S28,29} treatment for relativistic effects including spin-orbit coupling. The hybrid density functional approximation (DFA) PBE0^{S30} was used in combination with the all-electron ZORA/TZP^{S31} basis set and the NumericalQuality setting was set to good. NMR shifts (δ) were obtained by referencing the shielding constant of the calculated compound to a reference molecule. For ²⁹Si NMR, the shifts are given relative to tetramethylsilane (TMS). $\delta(^{35}\text{Cl})$ was predicted relative to NaCl in D₂O by calculating the chemical shift relative to CH₂Cl₂ and adding $\delta(\text{CH}_2\text{Cl}_2) = 232.3$ which was experimentally determined with NaCl in D₂O as the external standard.

$$\begin{aligned}\delta(^{29}\text{Si}) &= \sigma(\text{TMS}) - \sigma(\text{compound}) \\ \delta(^{35}\text{Cl}) &= \sigma(\text{CH}_2\text{Cl}_2) - \sigma(\text{compound}) + 232.3\end{aligned}$$

6.3. Scaling of calculated ^{35}Cl chemical shift values

Table S5. Experimentally determined (exp), calculated and scaled (scaled), as well as calculated, non-scaled (calcd) $\delta(^{35}\text{Cl})$ values of the endohedral Cl^- ions in selected silafullerenes. The calculated values were scaled according to the linear equation derived from the linear regression shown in Fig. S30.

Silafullerane	$\delta(^{35}\text{Cl})$		
	exp	scaled	calcd
$[\text{Cl}@Si_{20}\text{Cl}_{20}]^-$	126.0 ^{S32}	124.9	151.5 ^{S1}
$[\text{Cl}@Si_{20}(\text{SiBr}_3)_{12}\text{Br}_8]^-$ ([3] ⁻)	271.2	268.4	315.9
$[\text{Cl}@Si_{20}\text{H}_{12}\text{Cl}_8]^-$	273.8 ^{S32}	280.5	329.8 ^{S1}
$[\text{Cl}@Si_{20}(\text{SiCl}_3)_{12}\text{Cl}_8]^-$ ([A] ⁻)	274.5 ^{S32}	278.3	327.2 ^{S1}
$[\text{Cl}@Si_{20}(\text{SiBr}_2\text{H})_{12}\text{Br}_8]^-$ ([2] ⁻)	308.7	308.8	336.8
$[\text{Cl}@Si_{20}\text{H}_{20}]^-$	345.0 ^{S32}	340.8	398.8 ^{S1}
$[\text{Cl}@Si_{20}(\text{SiH}_3)_{12}\text{Cl}_8]^-$	363.7 ^{S1}	360.6	421.5 ^{S1}
$[\text{Cl}@Si_{20}(\text{SiH}_3)_{12}\text{Br}_8]^-$ ([4] ⁻)	372.9	371.2	433.7
$[\text{Cl}@Si_{20}(\text{SiH}_3)_{12}\text{Me}_8]^-$	457.1 ^{S1}	456.2	531.1 ^{S1}
$[\text{Cl}@Si_{20}(\text{SiH}_3)_{12}\text{H}_8]^-$ ([1] ⁻)	469.0 ^{S1}	472.2	549.4 ^{S1}

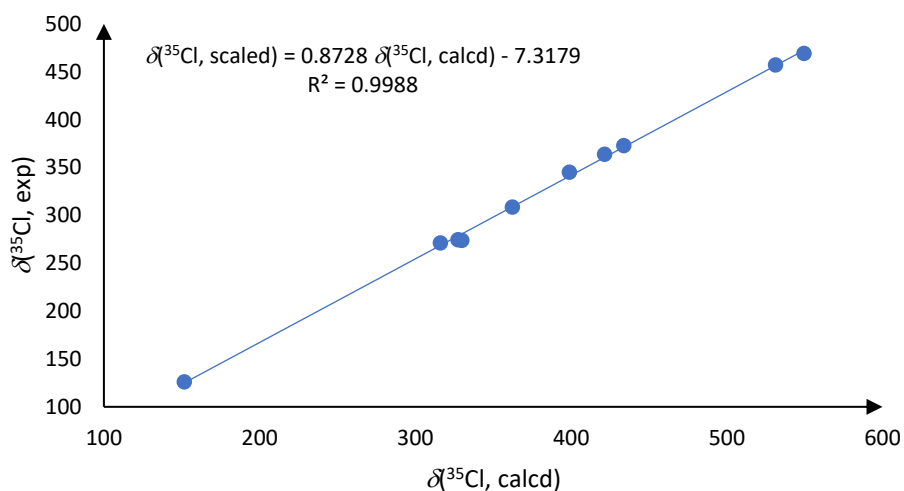


Figure S30. Linear regression of experimentally determined (exp) and calculated (calcd) $\delta(^{35}\text{Cl})$ values of the silafullerenes given in Table S5.

7. References

- S1 M. Bamberg, T. Gasevic, M. Bolte, A. Virovets, H.-W. Lerner, S. Grimme, M. Bursch and M. Wagner, *J. Am. Chem. Soc.*, 2023, **145**, 11440–11448.
- S2 G. R. Fulmer, A. J. M. Miller, N. H. Sherden, H. E. Gottlieb, A. Nudelman, B. M. Stoltz, J. E. Bercaw and K. I. Goldberg, *Organometallics*, 2010, **29**, 2176–2179.
- S3 The ^1H and $^{13}\text{C}\{^1\text{H}\}$ NMR spectra of C_6D_{12} in *o*DFB (1:5) were measured once with Me_4Si as an internal standard to determine $\delta(^1\text{H})$ of $\text{C}_6\text{D}_{11}\text{H}$ and $\delta(^{13}\text{C})$ of C_6D_{12} in this particular solvent mixture. These chemical shift values were used as references for the signals in all spectra subsequently measured using $\text{C}_6\text{D}_{12}/o\text{DFB}$ (1:5) as solvent.
- S4 M. Strohmalm, M. Hassman, B. Košata and M. Kodíček, *Rapid Commun. Mass Spectrom.*, 2008, **22**, 905–908.
- S5 M. Strohmalm, D. Kavan, P. Novák, M. Volný and V. Havlíček, *Anal. Chem.*, 2010, **82**, 4648–4651.
- S6 T. H. J. Niedermeyer and M. Strohmalm, *PLoS One*, 2012, **7**, e44913.
- S7 K. Hassler and G. Bauer, *J. Organomet. Chem.*, 1993, **460**, 149–153.
- S8 G. M. Sheldrick, *Acta Crystallogr. Sect. A Found. Crystallogr.*, 2015, **71**, 3–8.
- S9 G. M. Sheldrick, *Acta Crystallogr. Sect. C Struct. Chem.*, 2015, **71**, 3–8.
- S10 J. Wagler and R. Gericke, *Dalton Trans.*, 2017, **46**, 8875–8882.
- S11 https://photon-science.desy.de/facilities/petra_iii/beamlines/p24_chemical_crystallography/eh2/index_eng.html (accessed 2023-05-01).
- S12 V. A. Blatov, A. P. Shevchenko and D. M. Proserpio, *Cryst. Growth Des.*, 2014, **14**, 3576–3586.
- S13 A. L. Spek, *Acta Crystallogr. Sect. D Biol. Crystallogr.*, 2009, **65**, 148–155.
- S14 R. Rüger, M. Franchini, T. Trnka, A. Yakovlev, E. van Lente, P. Philipsen, T. van Vuren, B. Klumpers and T. Soini, ADF 2022.1, SCM, Theoretical Chemistry, Vrije Universiteit, Amsterdam, The Netherlands, <http://www.scm.com>, 2022 (accessed 2023-04-26).
- S15 F. Neese, *Wiley Interdiscip. Rev. Comput. Mol. Sci.*, 2012, **2**, 73–78.

- S16 F. Neese, F. Wennmohs, U. Becker and C. Riplinger, *J. Chem. Phys.*, 2020, **152**, 224108.
- S17 F. Neese, *Wiley Interdiscip. Rev. Comput. Mol. Sci.*, 2022, **12**, e1606.
- S18 S. Grimme, J. G. Brandenburg, C. Bannwarth and A. Hansen, *J. Chem. Phys.*, 2015, **143**, 054107.
- S19 H. Kruse and S. Grimme, *J. Chem. Phys.*, 2012, **136**, 154101.
- S20 S. Grimme, S. Ehrlich and L. Goerigk, *J. Comput. Chem.*, 2011, **32**, 1456–1465.
- S21 S. Grimme, J. Antony, S. Ehrlich and H. Krieg, *J. Chem. Phys.*, 2010, **132**, 154104.
- S22 A. V. Marenich, C. J. Cramer and D. G. Truhlar, *J. Phys. Chem. B*, 2009, **113**, 6378–6396.
- S23 F. Weigend, *J. Comput. Chem.*, 2008, **29**, 167–175.
- S24 F. Weigend, *Phys. Chem. Chem. Phys.*, 2006, **8**, 1057–1065.
- S25 G. Schreckenbach and T. Ziegler, *J. Phys. Chem.*, 1995, **99**, 606–611.
- S26 A. Klamt and G. Schüürmann, *J. Chem. Soc., Perkin Trans. 2*, 1993, 799–805.
- S27 C. C. Pye, T. Ziegler, E. Van Lenthe and J. N. Louwen, *Can. J. Chem.*, 2009, **87**, 790–797.
- S28 E. van Lenthe, E. J. Baerends and J. G. Snijders, *J. Chem. Phys.*, 1993, **99**, 4597–4610.
- S29 E. van Lenthe, E. J. Baerends and J. G. Snijders, *J. Chem. Phys.*, 1994, **101**, 9783–9792.
- S30 C. Adamo and V. Barone, *J. Chem. Phys.*, 1999, **110**, 6158–6170.
- S31 E. van Lenthe and E. J. Baerends, *J. Comput. Chem.*, 2003, **24**, 1142–1156.
- S32 M. Bamberg, M. Bursch, A. Hansen, M. Brandl, G. Sentis, L. Kunze, M. Bolte, H.-W. Lerner, S. Grimme and M. Wagner, *J. Am. Chem. Soc.*, 2021, **143**, 10865–10871.